Passenger Kinematics During Crash Avoidance Maneuvers

Matthew P. Reed
Sheila M. Ebert
B-K Daniel Park
Monica L.H. Jones

University of Michigan Transportation Research Institute

Final Report

UMTRI-2018-5

February 2018

Technical Report Documentation Page

1. Report No. UMTRI-2018-5	2. Government Accession No.	3. Recipient's Catalog No.
Passenger Kinematics During Crash Avoidance Maneuvers		5. Report Date
		6. Performing Organization Code
7. Author(s) Reed, M.P., Ebert, S.M., Park, B-K D., and Jones, M.L.H.		8. Performing Organization Report No.
9. Performing Organization Name and Address University of Michigan Transportation Research Institute 2901 Baxter Road Ann Arbor MI 48109		10. Work Unit No. (TRAIS)
		11. Contract or Grant No.
12. Sponsoring Agency Name and Address Toyota Collaborative Safety Research Center		13. Type of Report and Period Covered
		14. Sponsoring Agency Code
15. Supplementary Notes		

16. Abstract

Abrupt vehicle maneuvers that occur before a crash can affect occupant postures and may influence the level of protection provided by the occupant protection systems. Previous research has shown that occupant responses to on-road maneuvers have high variability, but the sample sizes have been too small for robust analysis of the potential effects of occupant characteristics such as age and body size. In addition, some studies have also suggested that participant awareness affects the magnitude of responses. To address these gaps, 87 men and women with a wide range of body size and age were recruited for a test track study. The purpose of the study was obfuscated somewhat by telling the participants that the study was focused on vehicle ride and handling. Testing was conducted at the University of Michigan's Mcity facility with the participants riding in the front passenger seat of a late-model sedan. Detailed anthropometric data were obtained from each participant, including 3D body scans. Vehicle motions were recorded with an inertial measurement unit and passenger head motions were tracked using a novel system based on a Microsoft Kinect sensor. During a short drive around the Mcity facility, participants answered questions about the vehicle ride until a they experienced an unaware, maximal braking event from 56 kph that peaked at approximately 1 g and lasted about 2 seconds. After the drive resumed, the participants experienced a sharp right turn with maximal braking, an abrupt lane change, and another maximal braking event. Based on video of facial reactions, nearly all participants were surprised by the first braking event.

The mean (standard deviation) of excursion of the estimated head center of gravity (CG) location in the first braking event was -135 (62) mm. The head CG excursion in the second braking event of -115 (51) mm was significantly less than in the first, but the difference was small relative to the within-condition variance. Head excursion on the second braking trial was less than on the first trial for 69% of participants. The maximum inboard head excursions in lane-change and right-turn maneuvers were -118 (40) mm and -131 (35) mm, respectively. Forward head excursions in braking were significantly smaller for older passengers and those with higher body mass index, but the combined factors accounted for less than 25% of the variance. Inboard head excursion in the lane-change event was significantly related to stature, but only about 7% of variance was related to body size. Head excursions for men and women did not differ significantly after accounting for body size. Global head angle changes during the events were generally smaller than 10 degrees and driven primarily by voluntary responses. Functional analysis methods were used to generate prediction corridors that can be used to tune and validate active human body models that are intended to simulate passenger response to pre-crash maneuvers. Future work should include a wider range of pre-crash posture and belt fit.

17. Key Words Crash safety, vehicle maneuvers, occupant motions	18. Distribution Statement		
19. Security Classif. (of this report)	20. Security Classif. (of this page)	21. No. of Pages 76	22. Price

Form DOT F 1700.7 (8-72) Reproduction of completed page authorized

Metric Conversion Chart

APPROXIMATE CONVERSIONS TO SI UNITS

SYMBOL	WHEN YOU KNOW	MULTIPLY BY	TO FIND	SYMBOL
LENGTH				
In	inches	25.4	millimeters	mm
Ft	feet	0.305	meters	m
Yd	yards	0.914	meters	m
Mi	miles	1.61	kilometers	km
AREA				
in^2	squareinches	645.2	square millimeters	mm^2
ft^2	squarefeet	0.093	square meters	m^2
yd^2	square yard	0.836	square meters	m^2
Ac	acres	0.405	hectares	ha
mi^2	square miles	2.59	square kilometers	km^2
VOLUME				
fl oz	fluid ounces	29.57	milliliters	mL
gal	gallons	3.785	liters	L
ft^3	cubic feet	0.028	cubic meters	m^3
yd^3	cubic yards	0.765	cubic meters	m^3
NOTE: volumes greater than 1000 L shall be shown in m^3				
MASS				
oz	ounces	28.35	grams	g
lb	pounds	0.454	kilograms	kg
T	short tons (2000 lb)	0.907	megagrams (or "metric ton")	Mg (or "t")
TEMPERATURE (exact degrees)				
°F	Fahrenheit	5 (F-32)/9 or (F-32)/1.8	Celsius	°C
FORCE and PRESSURE or STRESS				
lbf	poundforce	4.45	newtons	N
lbf/in^2	poundforce per square inch	6.89	kilopascals	kPa

LENGTH				
mm	millimeters	0.039	inches	in
m	meters	3.28	feet	ft
m	meters	1.09	yards	yd
km	kilometers	0.621	miles	mi
AREA				
mm^2	square millimeters	0.0016	square inches	in^2
m^2	square meters	10.764	square feet	ft^2
m^2	square meters	1.195	square yards	yd^2
ha	hectares	2.47	acres	ac
km^2	square kilometers	0.386	square miles	mi^2
VOLUME				
mL	milliliters	0.034	fluid ounces	fl oz
L	liters	0.264	gallons	gal
m^3	cubic meters	35.314	cubic feet	ft^3
m^3	cubic meters	1.307	cubic yards	yd^3
MASS				
g	grams	0.035	ounces	oz
kg	kilograms	2.202	pounds	lb
Mg (or "t")	megagrams (or "metric ton")	1.103	short tons (2000 lb)	T
TEMPERATURE (exact degrees)				
ºC	Celsius	1.8C+32	Fahrenheit	ºF
FORCE and PRESSURE or STRESS				
N	Newtons	0.225	poundforce	lbf
kPa	Kilopascals	0.145	poundforce per square inch	lbf/in^2

*SI is the symbol for the International System of Units. Appropriate rounding should be made to comply with Section 4 of ASTM E380.
(Revised March 2003)

ACKNOWLEDGMENTS

This research was supported by the Toyota Collaborative Safety Research Center. We thank Jason Hallman and Rini Sherony of the CSRC for their important contributions to this work. At UMTRI, a large number of staff and students contributed to the success of this project, including Annie Bonifas, Carl Miller, Laura Malik, Lindsay Sexton, Brian Eby, Brandon Waldron, Aditi Batra, Jessica Foss, Hannah Gannon, Juan Madrid, Spencer Miller, and Swetha Reddi.

CONTENTS

ABSTRACT

Abrupt vehicle maneuvers that occur before a crash can affect occupant postures and may influence the level of protection provided by the occupant protection systems. Previous research has shown that occupant responses to on-road maneuvers have high variability, but the sample sizes have been too small for robust analysis of the potential effects of occupant characteristics such as age and body size. In addition, some studies have also suggested that participant awareness affects the magnitude of responses. To address these gaps, 87 men and women with a wide range of body size and age were recruited for a test track study. The purpose of the study was obfuscated somewhat by telling the participants that the study was focused on vehicle ride and handling. Testing was conducted at the University of Michigan's Mcity facility with the participants riding in the front passenger seat of a late-model sedan. Detailed anthropometric data were obtained from each participant, including 3D body scans. Vehicle motions were recorded with an inertial measurement unit and passenger head motions were tracked using a novel system based on a Microsoft Kinect sensor. During a short drive around the Mcity facility, participants answered questions about the vehicle ride until a they experienced an unaware, maximal braking event from 56 kph that peaked at approximately 1 g and lasted about 2 seconds. After the drive resumed, the participants experienced a sharp right turn with maximal braking, an abrupt lane change, and another maximal braking event. Based on video of facial reactions, nearly all participants were surprised by the first braking event.

The mean (standard deviation) of excursion of the estimated head center of gravity (CG) location in the first braking event was -135 (62) mm. The head CG excursion in the second braking event of -151 (51) mm was significantly less than in the first, but the difference was small relative to the within-condition variance. Head excursion on the second braking trial was less than on the first trial for 69% of participants. The maximum inboard head excursions in lane-change and right-turn maneuvers were -118 (40) mm and -131 (35) mm, respectively. Forward head excursions in braking were significantly smaller for older passengers and those with higher body mass index, but the combined factors accounted for less than 25% of the variance. Inboard head excursion in the lane-change event was significantly related to stature, but only about 7% of variance was related to body size. Head excursions for men and women did not differ significantly after accounting for body size. Global head angle changes during the events were generally smaller than 10 degrees and driven primarily by voluntary responses. Functional analysis methods were used to generate prediction corridors that can be used to tune and validate active human body models that are intended to simulate passenger response to pre-crash maneuvers. Future work should include a wider range of pre-crash posture and belt fit.

INTRODUCTION

Approximately 40-50% of crashes are preceded by some sort of vehicle maneuver related to the crash event, such as braking or steering (Stockman 2016; Ejima et al. 2009). In these cases, the vehicle motion may cause occupants to move out of their initial positions, potentially into postures in which the occupant protection systems may be less effective in crashes. Current test procedures evaluate crash protection for a few extreme "out-of-position" scenarios, but the most tests and restraint optimizations are performed using anthropomorphic test devices (ATDs) that are "in-position", i.e., seated nominally.

Abrupt vehicle maneuvers prior to crashes may become more common as crash avoidance technologies that intervene to change vehicle movements become standard equipment on many vehicles in the coming decade. Automated emergency braking (AEB) for frontal crash avoidance is already available on many models, and major manufacturers have announced their intent to include AEB across their fleets. Manufacturers and suppliers have also demonstrated more advanced systems that are capable of rapid steering maneuvers to avoid crashes.

Although the benefits of these technologies for crash reduction and mitigation are beginning to be understood from test-track performance and field data, the effects of these rapid vehicle motions on unaware vehicle occupants have not been well quantified. When the maneuvers are successful in avoiding the crash, the consequences for the occupants are likely to be minimal. However, if a crash occurs in spite of the crash avoidance intervention, changes in occupant posture and position that result from the maneuvers may have an influence on the performance of the crash protection systems. Understanding the effects of changes in occupant posture that result from pre-crash maneuvers could have immediate benefit because driver-initiated maneuvers prior to crashes are already common.

Because the effects of pre-crash maneuvers on occupants could vary widely, methods for simulating these effects are needed. ATDs have been demonstrated to react unrealistically during vehicle motions typical of pre-crash maneuvers (e.g., Bohman et al. 2011). Consequently, computational human body models that are capable of representing a wide range of responses to vehicle maneuvers, including the effects of human muscle activations, are being developed (e.g., Ejima et al. 2009; Östh et al. 2012, 2014; Iwamoto et al. 2012; Östhmann and Jakobsson 2016). To support human model development and application, the focus of empirical research in this area has been on the kinematics and muscle responses of human volunteers.

Several previous studies have gathered data on occupant responses to aggressive vehicle maneuvers. Morris and Cross (2005) conducted a test-track study to investigate the motions of 49 "unaware" front-seat passengers during hard braking, lane changes, and other maneuvers. The testing employed subterfuge and distraction to reduce the participants' awareness of the purpose of the testing. Video was recorded of participants' reactions to maneuvers that began with the participants in various prescribed starting postures. Quantitative analysis of motions was not provided, but the authors reported a strong influence of lower-extremity bracing availability based on pre-maneuver posture.

Ejima et al. (2009) examined muscle activity and associated kinematics in low-speed frontal impacts on a sled. Five young men were tested on a rigid seat with their hands on a steering wheel. Hault-Dubrulle (2011) conducted a driving simulation study to examine responses to an impending collision. The authors documented bracing behaviors prior to simulated crashes, with

the occupants pushing against the steering wheel. These behaviors are not possible for passengers and may be unlikely for drivers operating in automated steering modes.

Bohmann et al. (2011) examined the responses of child passengers to vehicle maneuvers. The data demonstrated the strong influence of bracing with the feet on postural control. Schoeneburg et al. (2011) summarized passenger response data from a midsize male volunteer in hard braking. The level of awareness of the occupant was not reported.

Carlsson and Davidsson (2011) examined the responses of 17 men and women to hard braking as drivers and passengers. All were aware of the purpose of the study and had optical targets applied to their heads and chests. Forward excursions for passengers were similar for both automated and driver-initiated braking. The locking of the seatbelt approximately 500 ms into the event appeared to be the primary factor limiting torso and head movement. Peak head excursions were larger for women than for men at the same stature, but the range of responses was more than 100% of the mean.

Östh et al. (2013) and Ólafsdóttir et al. (2013) reported an extensive study of occupant responses to automated braking events of approximately 1.1g for both drivers and passengers, respectively. The bracing behaviors reduced excursions for drivers, and a seatbelt equipped with a reversible pre-tensioner reduced excursions for both drivers and passengers. The participants in this study were well aware of the purpose of the testing and were instrumented for motion tracking and electromyography. The 11 men and 9 women who participated in the passenger trials were tested first in the driver seat. The data showed a large amount of variability in excursions due to braking. The range of peak head excursions was about 200% of the mean value.

Kirchbichler et al. (2014) measured front passenger motions in a range of braking and lane-change maneuvers with a total of 51 men and 6 women. The vehicle was equipped with a passive optical motion capture system and participants wore a specially designed suit with markers. The first test series was conducted with a flat rigid seat and a lap belt only. The second series included a more realistic seat. Some trials are described as “unaware” in the sense that the participants were not explicitly warned that the maneuver was about to begin. However, the overall level of test preparation was high, so that the initial state of the participant may have been quite different from a typical vehicle passenger.

Huber et al. (2015) presented additional data from the Kirchbichler et al. test series, focusing on data from 19 men and 6 women in braking and lane-change-with-braking maneuvers. The data collection methods and limitations were the same as those presented by Kirchbichler the previous year. The data demonstrate a large amount of variability between individuals, such that the range ±1SD spans more than 50% of the mean forward excursion for hard braking events. For head angle change, 2 SD is greater than the mean change from the starting posture.

This review of the literature demonstrated several gaps in the existing knowledge of occupant responses to sudden vehicle maneuvers:

- More data are needed to characterize the responses of minimally aware occupants. The available data demonstrate that awareness reduces excursions, so the boundary cases for restraint system design are not meaningfully represented in the responses of aware occupants.

- More data are needed for passengers in realistic vehicle seating scenarios. The Kirchbichler et al. data used unrealistic seating scenarios as well as a relatively artificial test conditions (e.g., participants wore a Lycra suit).

- More data are needed from a diverse occupant pool. The limited data available to date suggest that occupant size, gender, and age may all affect responses. If the boundary cases for restraint design are older women, the currently available data are insufficient. Because the range of responses observed in previous studies is so large, there is a need to understand the extent to which the response can be predicted from occupant attributes and to identify the subgroups that experience the largest excursions.

This report presents the methods and results of a study aimed at addressing these gaps. The study is differentiated from previous work in several ways:

- We developed a methodology designed to obtain an initial response that was as close to "unaware" as is feasible within an ethical experimental paradigm. We repeated the initial exposure to evaluate the effects of habituation during the testing.

- We used a large, diverse subject pool to enable robust statistical assessment of the effects of passenger characteristics on kinematics.

- We applied a new head-tracking method developed at U-M to provide fast, accurate tracking of kinematics, enabling testing of large numbers of subjects without requiring a large amount of manual tracking or an intrusive tracking system.

METHODS

Vehicle and Instrumentation

The test vehicle was a 2016 Toyota Avalon sedan with the Limited trim level, which included leather seats. The vehicle was equipped with a four-wheel anti-lock braking system and disc brakes front and rear. Figure 1 shows the outside of the vehicle and Figure 2 shows interior views of the right front passenger area.

An HD PRo Webcam C920 (PN 960-000764) was mounted to the headliner of the vehicle to monitor foot position, and a MicroStrain 3DM-GX5-10 inertial measurement unit (IMU) was installed near the mass center of the vehicle to quantify the acceleration and rotation rates of the vehicle during events. During testing, data were recorded from the IMU at 100 Hz and the camera data were recorded at 30 frames per second. Figure 3 shows the view of the footwell.

Figure 1. 2016 Toyota Avalon Limited test vehicle.

Figure 2. Front passenger seating area with seat set to the lowest position, flattest cushion angle, and a back angle of 23 degrees (SAE J826) and moved fully rearward on seat track.

Figure 3. Web camera field of view

Participants

Eighty-seven adults (44 women and 43 men) participated in the study. Table 1 lists summary statistics for anthropometric variables and Figures 4 through 6 show distributions. Participants age range was eighteen to seventy years with a mean of 45 years, and 37 of the participants were 55 years or older. Participant BMI range was 19 to 67 kg/m^2 with a mean of 29 kg/m^2, and 34 of the participants had a BMI over 30 kg/m^2. Participant stature range was 1482 mm to 1929 mm.

Table 1. Summary statistics for participant pool

	BMI < 30 kg/m^2	BMI >= 30 kg/m^2	Age < 55 years	Age >= 55 years	Total
Female Participants	27	17	23	21	44
Mean (SD)	24.5 (3.1)	39.4 (8.6)	30.7 (10.3)	62.1 (3.4)	
Male Participants	27	16	27	16	43
Mean (SD)	24.6 (3.1)	35.4 (5.2)	32.5 (11.3)	62.1 (4.9)	
Total	53	34	50	37	87

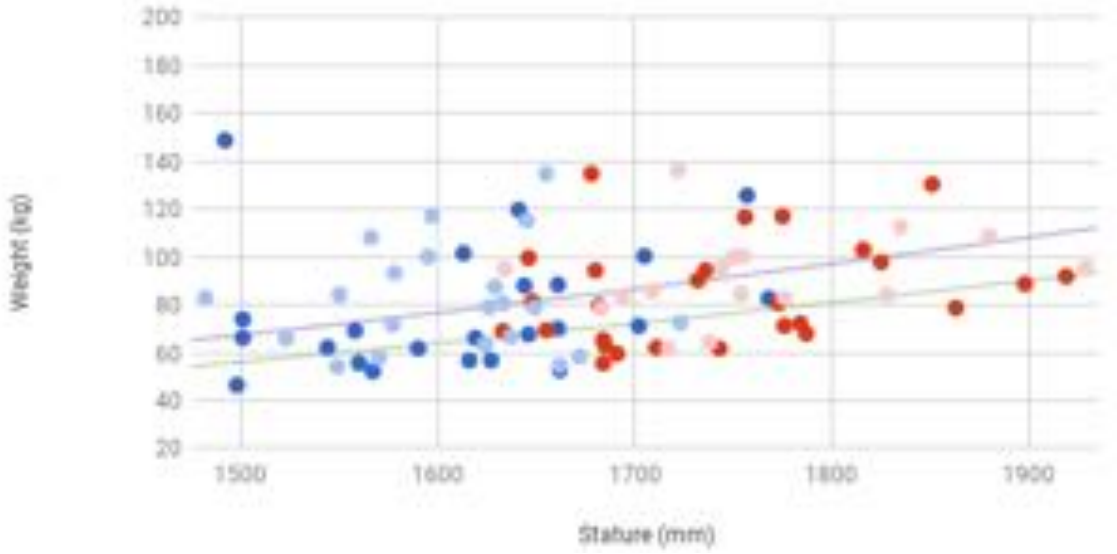

Figure 4. Weight by stature for male (red) and female (blue) participants. Color density is proportional to age.

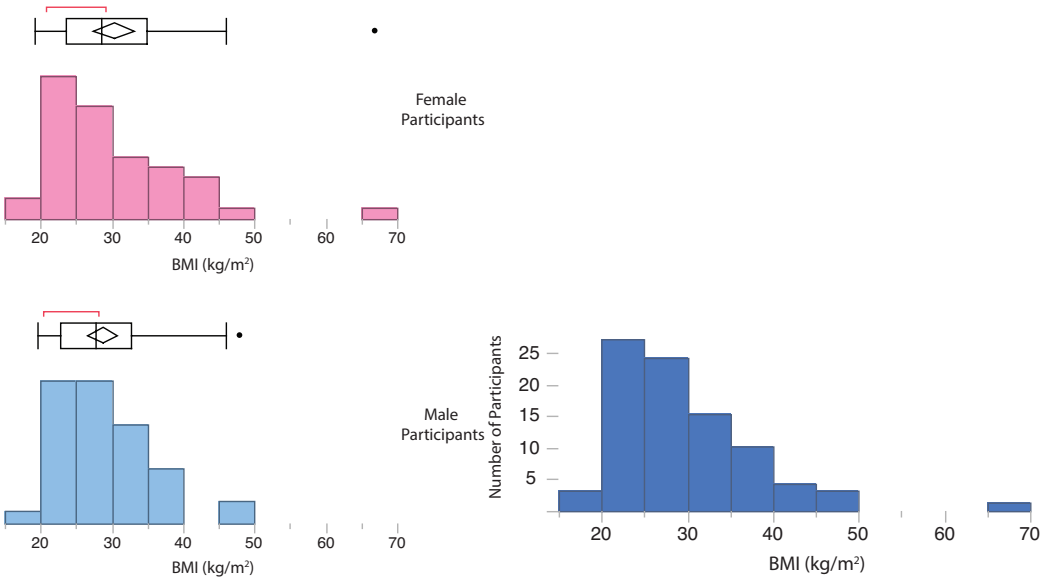

Figure 5. Histograms of BMI for female, male, and all participants.

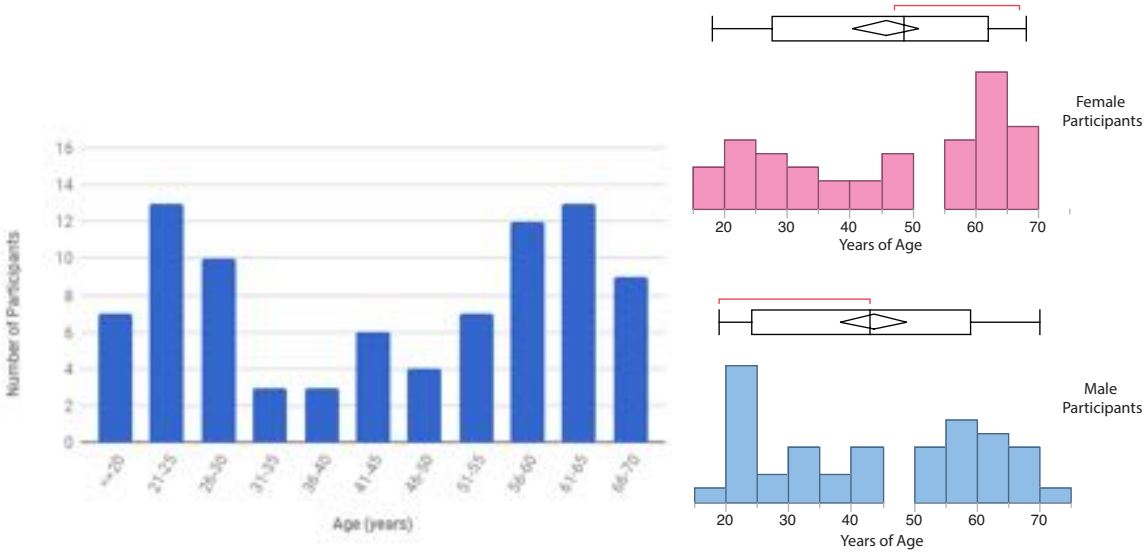

Figure 6. Participant age distribution.

Data Collection Sequence

The study protocol was approved by an Institutional Review Board at the University of Michigan (Approval HUM00120296). Figure 7 shows the sequence of data collection for each participant. After written informed consent was obtained, detailed anthropometric data were obtained using

standard and three-dimensional methods. The participant sat in the right front passenger seat of the test vehicle at UMTRI and then was driven to the Mcity facility for testing.

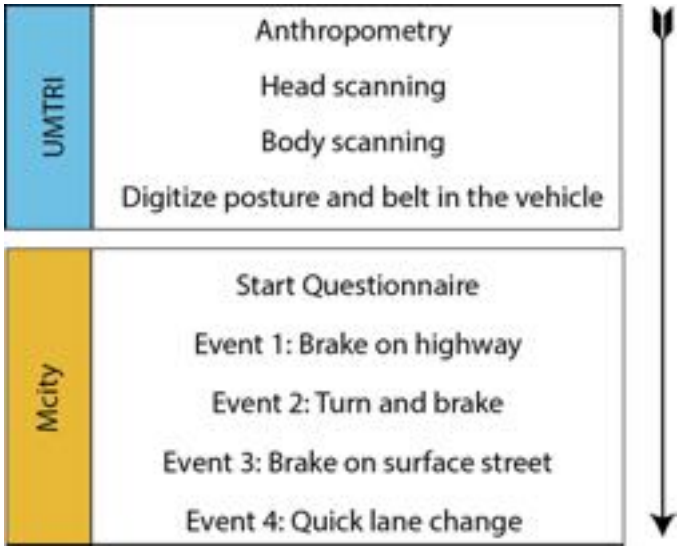

Figure 7. Data collection sequence.

Anthropometry

Standard anthropometric dimensions, including stature, body weight, and linear breadths and depths were gathered from each participant to characterize the overall body size and shape. Table 2 contains a complete list of measurements. Figure 8 illustrates the measurement of two head dimensions. All dimensions were obtained minimally clad, except that stature was measured with and without footwear to characterize heel height.

Table 2. Standard anthropometric variables

Gender	Tragion to top of head
Date of birth	Head breadth
Stature (with shoes)	Head length
Stature (without shoes)	Maximum hip breadth
Weight (without shoes)	Buttock-knee length
Erect sitting height	Bi-acromial breadth
Eye height (sitting)	Shoulder breadth
Shoulder height (sitting)	Bi-ASIS breadth
Knee height	

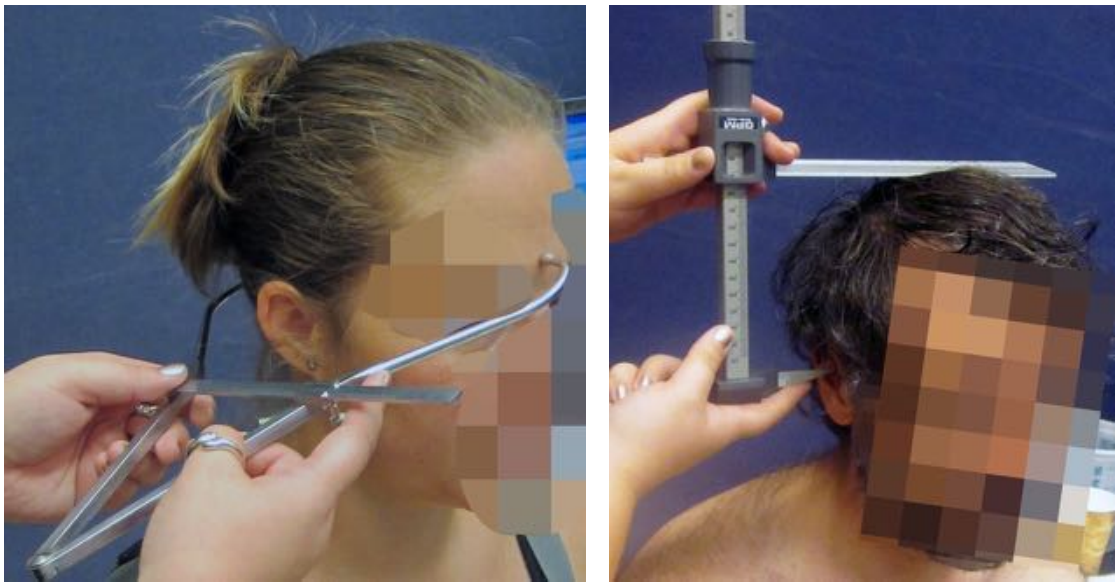

Figure 8. Examples of measuring standard anthropometric dimensions: head length (left) and tragion to top of head (right).

Hardseat

Body landmark locations were recorded in the laboratory hardseat shown in Figure 9. The hardseat allows access to posterior spine and pelvis landmarks that are inaccessible in the automotive seat. The adjustment for adiposity described in Reed et al. (2013) was applied to the points recorded on the pelvis (Figure 10). The hardseat has a 14.5˚pan angle and a 23˚ back angle designed to produce postures similar to those in an automotive seat. Table 3 lists the landmarks recorded in the hardseat.

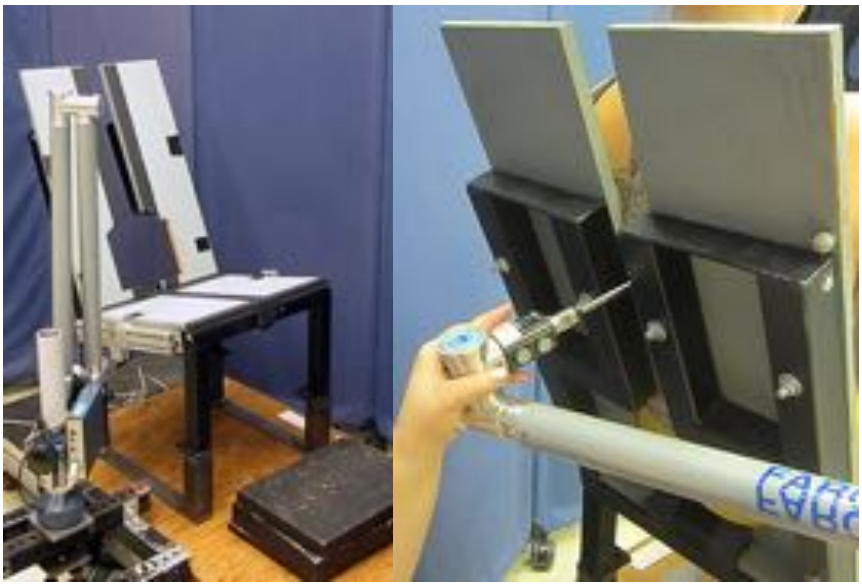

Figure 9. Hardseat with back opening (left) that allows access to posterior spine and pelvis as shown in center photo. Example of head IMU location being digitized with FARO Arm (right)

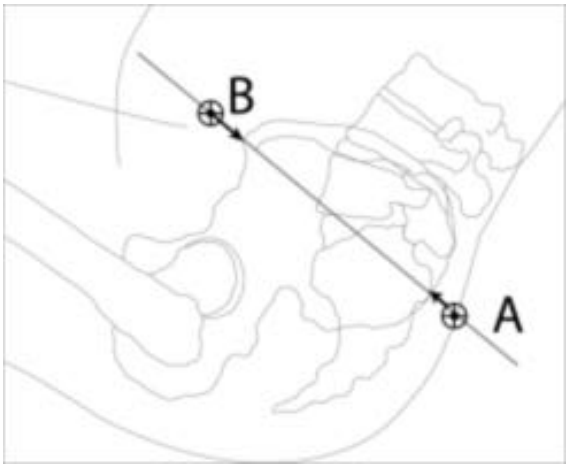

Figure 10. Compensation for adiposity at the PSIS flesh margin (A) and ASIS flesh margin (B) separating the depressed surface landmark from the underlying bone landmark (see Reed et al. 2013).

Table 3. Landmarks, head targets, and head points digitized in hardseat

Back of head	Suprasternale	C7
Top of head (vertex)	Substernale	T4
Tragion, Rt and Rt	Lateral femoral epicondyle, Lt and Rt	T8
Ectoorbitale, Lt and Rt	Medial femoral epicondyle, Lt and Rt	T12
Infraorbitale at pupil center, Lt and Rt	Suprapatella, Lt and Rt	L1
Glabella	Infrapatella, Lt and Rt	L2
Cheekbone marker, Lt and Rt	Heel, Rt	L3
Temple marker, Lt and Rt	Lateral malleolus, Rt	L4
Hairline marker, Lt and Rt	Medial malleolus, Rt	L5
Above glabella marker	Lateral ball of foot, Rt	ASIS, Lt and Rt
Anterior acromion, Lt and Rt	Medial ball of foot, Lt	PSIS, Lt and Rt
Lateral humeral epicondyle, Lateral, Rt	Toe (longest tibiale), Lt and Rt	
Ulnar styloid process, Rt		

Head Scanning

Head shape and surface contours were recorded using a 3D Systems Sense hand-held, infrared depth scanner (Figure 11). Figure 12 shows examples of the head scan data. Prior to scanning, the reference points listed in Table 4 were placed on the participant's forehead and face using non-toxic paint (Figure 13). The location of the head landmarks and head tracking targets listed in Table 5 were manually digitized on the head scans using Meshlab software (Figure 14).

Figure 11. Scanning a participant's head with the hand-held scanner.

Figure 12. Examples of head scans with color texture (left and center) and without (right).

Figure 13. Locations of the head targets as seen in a head scan.

Table 4. Head-tracking target locations

Target	Location
1	Above glabella on the centerline of the face, above where the brow moves with facial expression
2 & 3	On temples, anterior of the hairline (left and right)
4 & 5	Higher on the forehead making a triangle with glabella and temple stamps, placed as superiorly as possible without being covered by hair (left and right)
6 & 7	On the cheekbone, at the tragion height, as far anterior as possible, posterior to skin movement caused by facial expressions (left and right)

Table 5. Landmark and target points digitized in head scans

Landmarks	**Head Tracking Targets**
Back of head	Cheekbone, Lt and Rt
Top of head	Temple, Lt and Rt
Gonion, Lt and Rt	Near hairline, Lt and Rt
Tragion, Lt and Rt	Above glabella
Ectoorbitale, Lt and Rt	
Infraorbitale at center of eye Lt and Rt	
Glabella	
Tip of nose	
Tip of chin (mentum)	
Gonion, Lt and Rt)	
Infrathyroid	

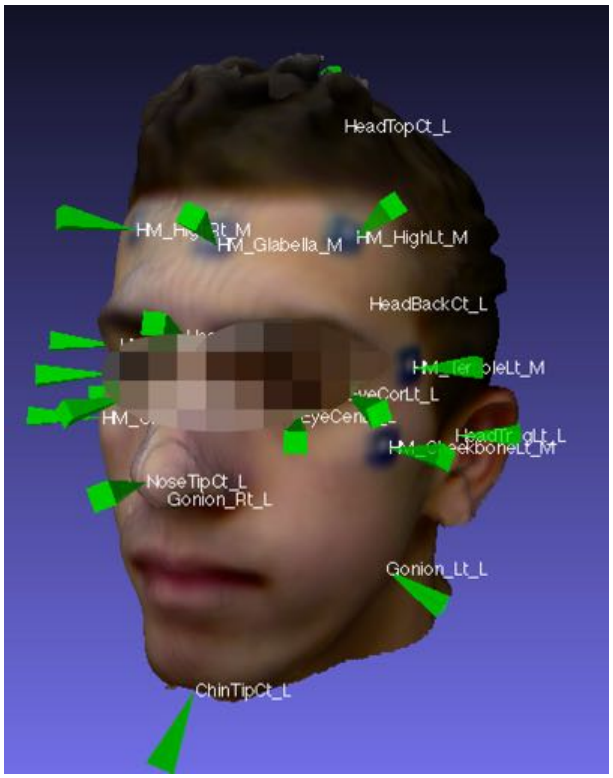

Figure 14. Example of landmarks and head targets digitized in head scans, shown in the Meshlab software used to digitize the points.

Body Scanning

Body shape and surface contours were recorded using a Vitronic Vitus XXL full-body laser scanner and Scanworx software by HumanSolutions. The VITUS XXL records hundreds of thousands of data points on the surface of the body in about 12 seconds by sweeping four lasers vertically. The two cameras on each of the four scanning heads record the laser light contour projected on the participant and translate the images into three-dimensional point data. Figure 15 shows a participant being scanned.

The participants were scanned in range of postures that included standing, unsupported seated, seated driving, and several other postures that spanned three recline angles. Figures 15 and 16 illustrate these two of these postures.

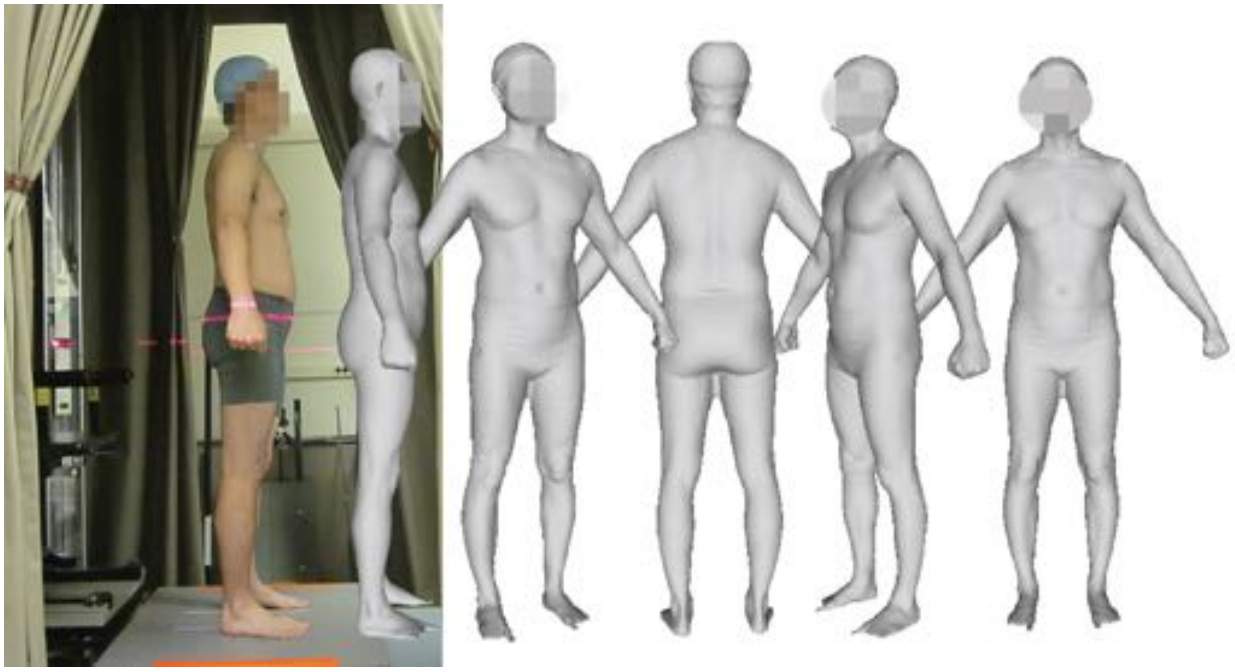

Figure 15. Participant scanned in T2 posture.

Figure 16. Participants scanned in passenger posture (CB).

In-Vehicle Postures

Each participant sat in the front passenger position of the test vehicle. The investigator instructed the participants to move all the way back in the seat, and then rock side-to-side a couple of times to "get comfortable," and then slide their feet forward and rest them on their heels. The participants were instructed to rest their palms on their thighs and relax their shoulders. The investigator asked the participants to not use the armrests initially unless the size of the participant required that they had to actively lift their arms to avoid them.

Before placing their arms in the standard posture, the participant put on the seat belt and the investigator adjusted the D-ring height to center the shoulder belt on the participant's clavicle (this location was subsequently recorded – see below). The investigator then instructed the participant to tighten the seat belt by pulling up on the shoulder belt near the buckle. If the participant did not tighten the belt or did not place the lap portion of the belt low on the pelvis, the investigator moved the belt and pulled it so that it was snug. Targets were placed on the seat belt webbing where it crossed the sternum, clavicle, and midline of the pelvis (Figure 17). Other targets were placed along the lap and shoulder belt at locations that were visible to the Kinect camera. Participants were asked to keep the head in an "alert position" (Figures 18 and 19) while the investigator recorded the posture and the location of the seat belt with a FARO Arm (Figure 20). Figure 21 shows a participant ready for testing with the questionnaire taped to her thighs. The tape was used to preclude the participant lifting the questionnaire and blocking the camera views. Table 6 lists the points recorded to quantify the initial posture, position, and belt fit.

Table 6. Points and streams digitized in the vehicle

Participant	Vehicle
C7 (Cervicale)	3 Points on door opening frame
Back of head (max rearward)	
Top of head (max height)	Seat
Tragion, Rt	Seat pan reference points
Ectoorbitale, Rt	Seat back reference point
Infraorbitale at pupil center, Rt	
Glabella	Restraint System
Stamp targets on head (4)	D-ring reference point
Suprasternale	Buckle reference point
Substernale	
Medial clavicle, Rt	Shoulder Belt
Lateral clavicle, Rt	Inboard and outboard edge on clavicle
Anterior of acromion, Rt	Top and bottom edge at participant's midline
Lateral humeral epicondyle, Rt	
Lateral ulnar styloid process, Rt	Inboard edge at participant's Suprasternale height
ASIS, Lt and Rt	
Suprapatella,Lt and Rt	Quad target locations (4)
Infrapatellat Lt	
Lateral femoral epicondyle Rt	Lap Belt
Medial femoral epicondyle Lt	Top edge and bottom edge at ASIS lateral position (Lt and Rt) and at participant's midline
Toe (bottom edge of sole, longest shoe point), Rt	
Lateral ball of foot, Rt	
Heel (bottom edge of sole at midline), Rt	Quad target locations (3)
Lateral malleolus, Rt	
	Seat Belt Streams
Stream of points along a sagittal line running anteriorly from shoulder to knee	Top/ inboard edge of the shoulder belt from latch plate to D-ring
	Top edge of the lap belt from latch plate to as close to the lower outboard anchor as possible

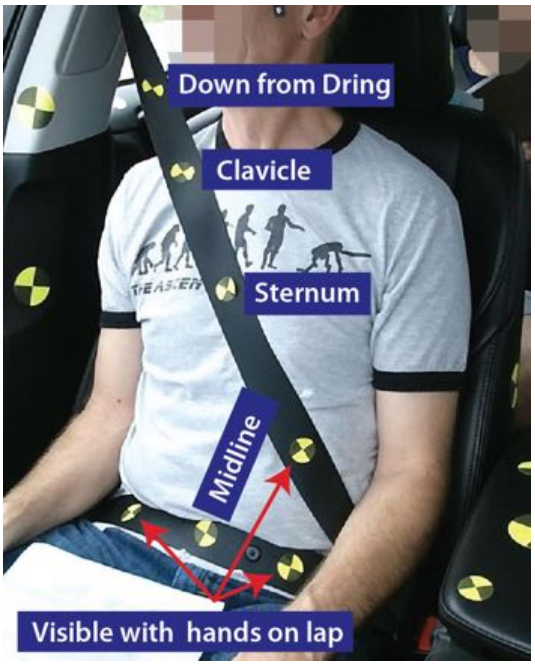

Figure 17. After the participant donned the seat belt quad targets were placed on the webbing where it crossed the sternum, clavicle, and midline of the pelvis. Other targets were placed along the lap and shoulder belt at locations that were visible to the Kinect camera.

Figure 18. Examples of female participants in initial posture in test vehicle.

Figure 19. Examples of male participants in test vehicle

Figure 20. Investigator using FARO Arm to digitize points on participant, vehicle, and belt

Figure 21. Testing posture: feet slid forward on heels and hands on thighs; questionnaire taped to thighs to prevent participant lifting it and blocking Kinect camera.

Occupant Kinematics Data

The primary data collection system was based on a Microsoft Kinect version 2 sensor. The Kinect sensor was positioned near the center of the dashboard facing the passenger seat as shown in Figure 22. The orientation of the sensor was chosen to capture upper-body and head movements. Figure 23 shows a screenshot of the data collection system recording raw Kinect data as well as webcam data and IMU data simultaneously. The program records the Kinect raw data records containing 512 × 424 px depth data, 1920 × 1080 px RGB data at 30 Hz during the events. Linear and rotational accelerations of the vehicle were recorded from the IMU at 100 Hz. Timestamps in milliseconds were recorded for each frame. To synchronize the IMU data to the Kinect data, the IMU data were linearly interpolated based on the timestamps to match to the Kinect frames.

Figure 22. Kinect RGB camera field of view

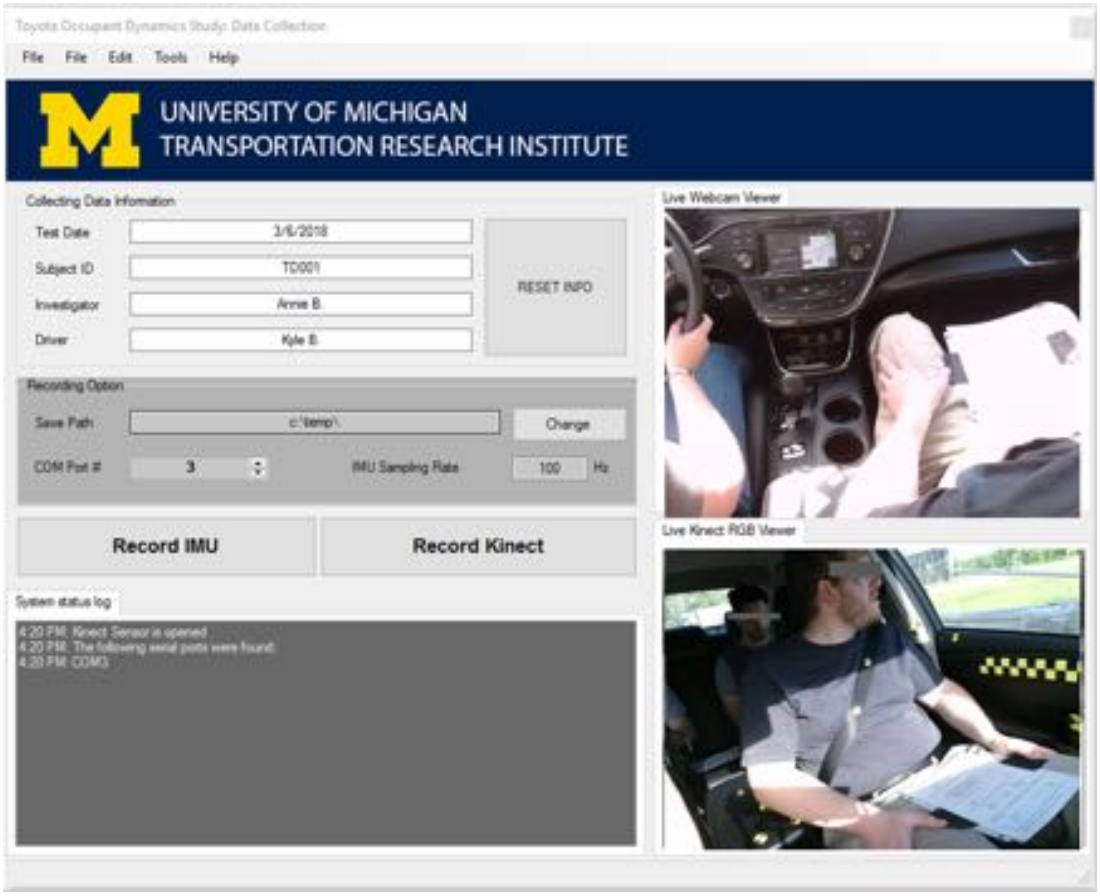

Figure 23. A screenshot of the data collection program interface.

Depth Data Processing

Recorded depth data were converted to 3D point cloud data. Table 7 shows the intrinsic parameters of the Kinect V2 sensor applied to convert the depth data while minimizing the tangential and radial distortions by the lens. By the nature of a time-of-flight depth sensor, "flying pixel" artifacts are observed close to depth discontinuities (Gottfried, et al., 2014). Since the artifacts degrade the fitting quality and performance, they were removed from the point cloud data using a simple filter. This filter selects the artifact points based on the nature that these points have less surrounding point density. By eliminating points that has less than a certain number of neighboring points within a radius, these artifacts can be removed

The standard video color images containing red, green, and blue (RGB) data were calibrated to the depth image space using the Kinect software development kit (SDK) supplied with the sensor to find the corresponding depth pixels and applied to the converted depth points. Finally, the point data were transformed to match the vehicle coordinate system by aligning depth points of the unoccupied vehicle space to the vehicle coordinate system, in which X is rearward, Z is upward, and the origin is located at the H-point of the passenger seat with the seat in the test position (full rear). Figure 23

shows an example of processed depth point cloud with RGB data and the effect of the flying-pixel artifact filtering.

Table 7. Camera intrinsic parameters for Kinect calibration

Parameter Name	**Value**
Focal Length X	366.7479
Focal Length Y	366.7479
Principal Point X	258.0758
Principal Point Y	208.6287
Radial Distortion 2nd order	0.08606404
Radial Distortion 4th order	-0.272878
Radial Distortion 6th order	0.0977018

Figure 24. Processed Kinect depth data with RGB. Before (left) and after (right) flying pixel artifact filtering.

Kinect Depth Data Accuracy

A camera calibration board (590 mm x 680 mm) was used for estimating the depth accuracy in the space of interest. The board was placed in different locations as shown in

Figure 25 and measured using both FARO Arm and Kinect sensor. Depth and color data obtained from the Kinect sensor were converted to 3D point cloud data using the software supplied with the Kinect. Ten Kinect depth frames per trial were used to minimize noise effects using a method developed previously (Park et al. 2015).

Figure 26 shows a total of 68 points on the board digitized using FARO Arm. To match the coordinate systems between FARO Arm and Kinect systems, the frontal surface of the Kinect device and the lens location were also digitized as well as the board. The same set of points were manually digitized from the processed Kinect depth data and compared with these FARO Arm points.

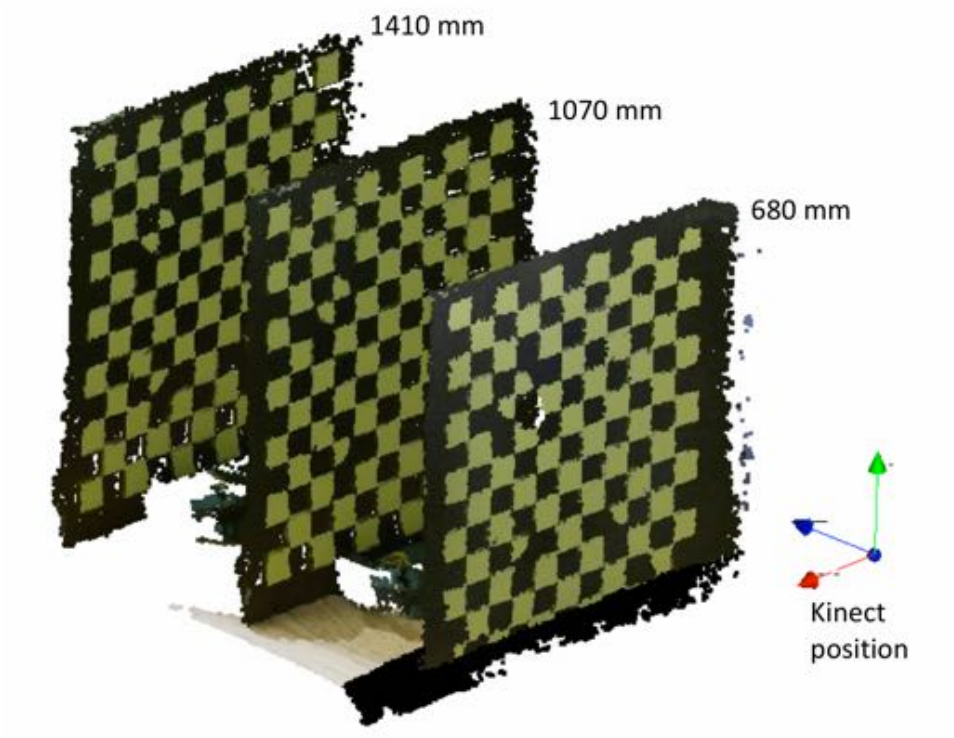

Figure 25. Kinect depth data of a calibration board in different locations.

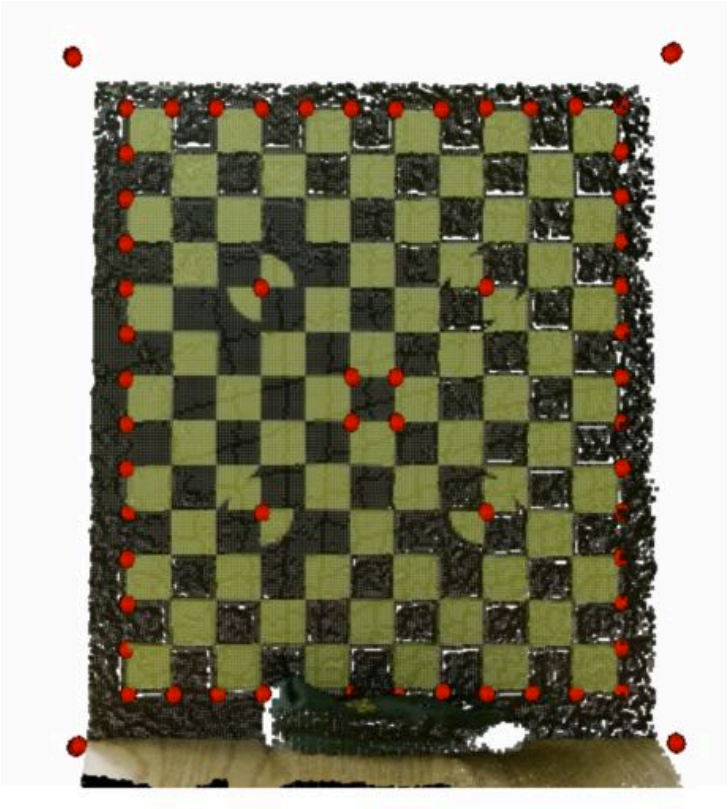

Figure 26. Digitized points using FARO Arm (red points) on an aligned Kinect depth data

Table 8 shows comparisons between FARO Arm digitized points and Kinect depth data of the calibration board. Kinect depth data shows consistent errors across the different distances. The mean error ranges 1.7 mm to 2.3 mm and the root-mean-squared-error ranges 2.1 mm to 3.0 mm. From a visual inspection, noise tends to be larger in areas with darker color.

Table 8. Comparisons of the digitized board points between FARO Arm and Kinect

Distance to sensor	**Mean**	**50th %**	**95th %**	**RSME**
680 mm	2.3 mm	1.8 mm	5.8 mm	2.9 mm
1070 mm	2.1 mm	1.5 mm	8.1 mm	3.0 mm
1410 mm	1.7 mm	1.5 mm	3.7 mm	2.1 mm

In addition to the accuracy assessment using the grid, an ATD head was used to evaluate the Kinect data accuracy for measuring head geometry and location. Figure 27 shows

ATD head placements chosen to be in the range of possible occupant head locations. Kinect depth data were captured as well as the FARO Arm data and processed in the same manner as the grid data. Four markers on the ATD head were digitized using FARO Arm. A 3D scan of the head was aligned to these digitized markers and compared with the Kinect depth data.

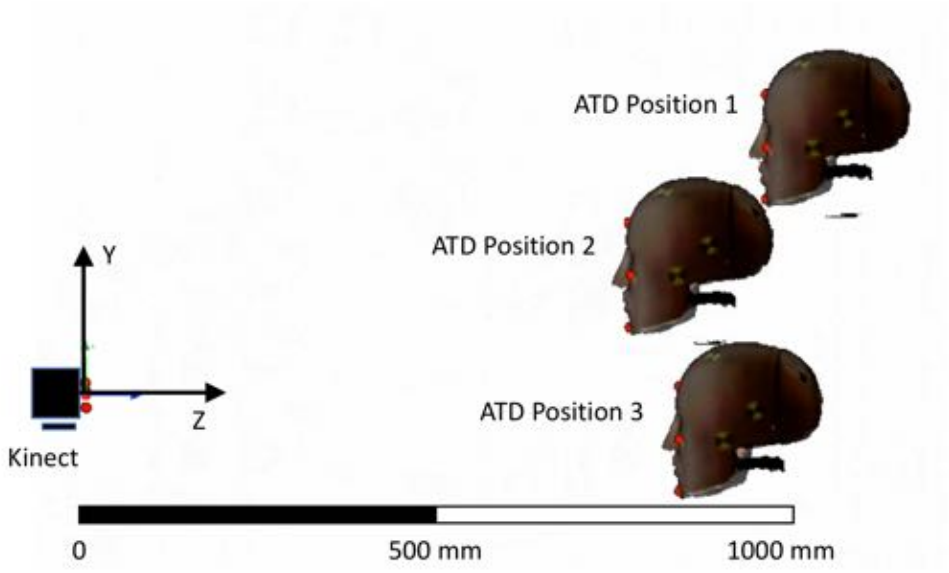

Figure 27. ATD head placements covering possible occupant head locations relative to the sensor.

Figure 28 shows the comparison between the Kinect depth data and the 3D scan aligned to the digitized FARO Arm points of the ATD head. The error level was about the same with the comparison of the calibration board. Kinect depth data showed a good accuracy in measuring both the shape and distance of the target ATD head. The mean error showed good consistency with a range of 2.0 mm to 2.6 mm relative to the measurements using the FARO Arm coordinate digitizer.

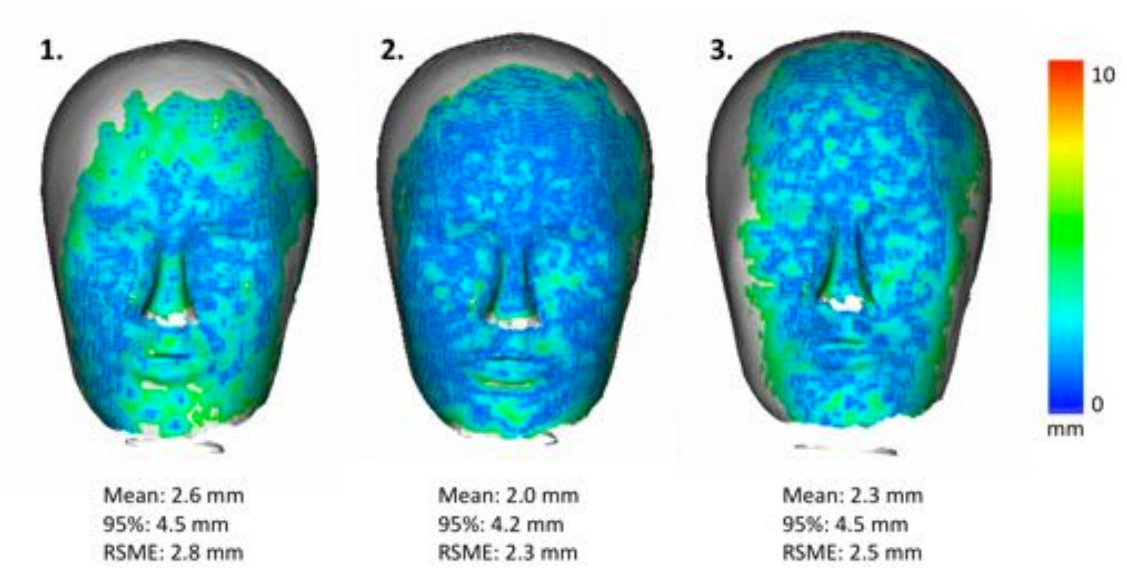

Figure 28. Illustration of measurement errors using ATD head in a range of positions (see Figure 27).

Head Fitting

The scanned head model was fit to the processed depth data to estimate the head location and orientation frame by frame. The scanned head model was first decimated to reduce the number of surface points and trimmed to represent only the part of the head and face typically visible in the Kinect data. For the first frame, a 2D face detection algorithm using Haar feature-based cascade classifiers (Paul and Jones, 2001) was employed to obtain an initial guess of the head position from an initial 2D image. A trained cascade classifier for this face detection was obtained from OpenCV library (opencv.org). When the face area was detected in the 2D color image, corresponding 3D points were selected, and the head model was translated to the mean position of the selected points.

An iterative closest point (ICP) method was used to fit the head scan to the depth points. To reduce computational time, only the points close to the head scan surface were considered as candidates for the ICP. A *kd*-tree was built on the candidate depth points to rapidly find the correspondences between the head scan vertices and the depth points. After the scan points were paired with the closest points among the depth points, the ICP was applied to estimate a transformation from the scan points to the paired depth points.

The ICP fitting performance was further improved by applying an adaptive criterion to reduce the number of point pairs, such that scan-depth point pairs separated by a distance over a set value were ignored (Figure 29). When a longer distance criterion is used, more point pairs are considered in the ICP so that a rapid jump can be made in an iteration at the cost of a relatively large fitting error. This is useful when the distances between scan points and the depth points are large. In contrast, the small distance criterion is appropriate for detailed geometric fitting, but the convergence is slow. In this study, the criterion distances varied from 100 mm to 10 mm over iterations according to 90th percentile distances of the initial pairs, and the iteration number was determined by the

convergence rate in the range of 20 ~ 100. The ICP was terminated when the amount of transformation in the previous timestep fell below a set threshold.

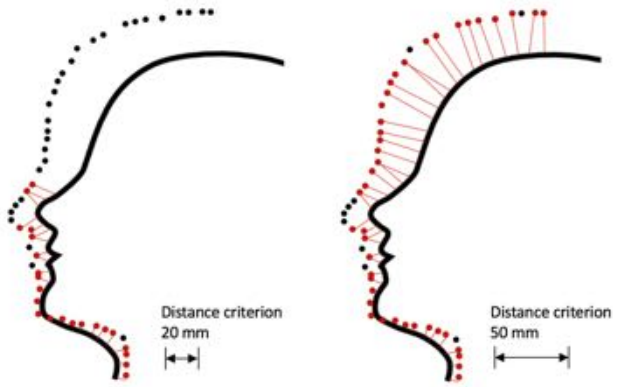

Figure 29. Selected source-target pair (in red) with different distance criteria (dotted: depth points, solid: scan surface)

The fitted head location for a given frame was used as an initial guess for the fitting of the next frame. The average fitting time was 0.57 second per frame on a desktop computer (Intel i7 3.6 GHz processor, 32GB RAM).

Finally, all the transformation matrices of the fitted head were interpolated using a radial basis function (RBF) with the Gaussian basis to resample the data while smoothing the position and orientation trajectories. In this interpolation, the RBF transfers time variables to transformation matrices so that a transformation matrix at an arbitrary time can be estimated.

Verifying Head Tracking

Head tracking performance using the Kinect system was verified by comparison to 3D tracking obtained using video data from multiple cameras. This analysis is reported in detail in Park et al. (2017). In pilot testing for the current project, the Kinect system was paired with three grayscale video cameras operating at 30 Hz. A target on the forehead was tracked semi-manually using the video data and TEMA software (Image Systems, Linköping, Sweden).

Figure 30 shows the comparison of the displacement of the landmark on the forehead of one subject for two events. The mean discrepancy between the TEMA and Kinect results was 2.4 mm and the 95th%tile discrepancy was 5.9 mm for the braking event. For the lane changing event, the mean discrepancy was 3.9 mm with a 95th%tile of 9.4 mm.

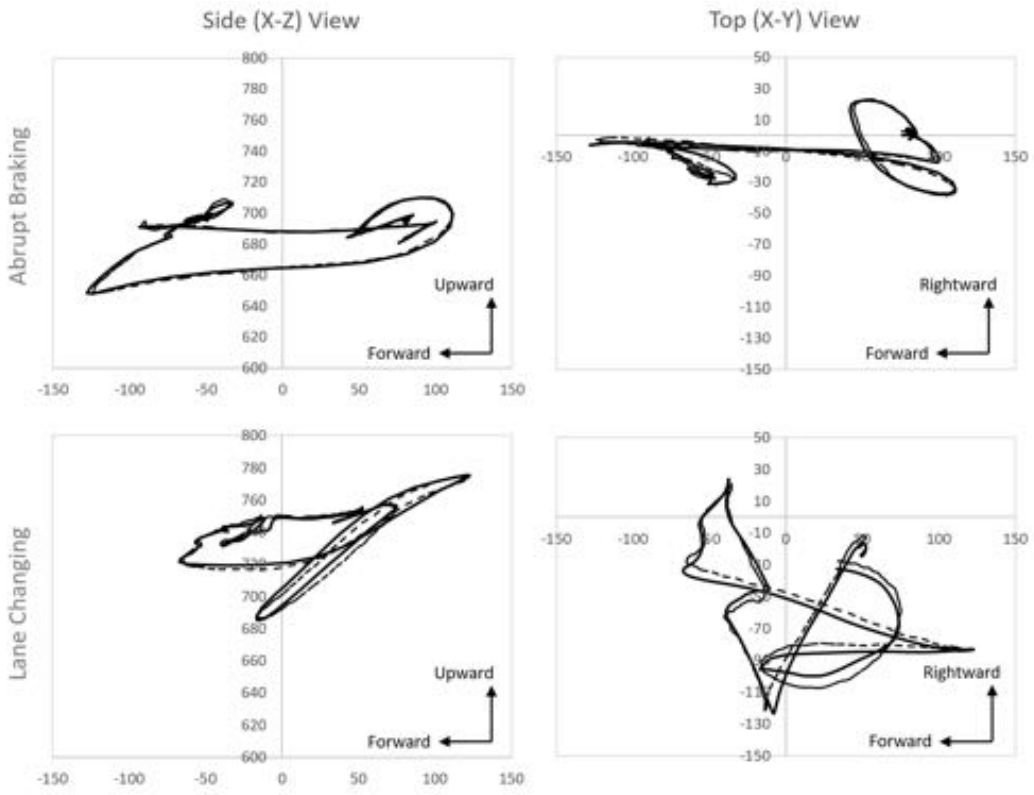

Figure 30. Comparison of landmark tracking using TEMA (dashed lines) and the Kinect-based system (solid line) for two events.

Tracking Head Landmarks, Center of Gravity Location, and Orientation

The transformation matrix calculated for each Kinect frame was applied to the head/face landmark points digitized from the head scan, giving landmark trajectories throughout the event. A head coordinate system was established with the origin at the midpoint between the tragion landmarks. The head lateral (Y) axis was established passing from the left to right tragion landmarks. The head vertical (Z) axis was obtained perpendicular to the plane formed by the y axis and the left infraorbitale. The fore-aft (x) axis was computed as the cross product between the Y and Z axes. The midsize-male head center of gravity (CG) location from Schneider et al. (1983) was used to estimate the head CG location at a point 8 mm forward and 35 mm above the head origin in the head coordinate system. (Note that the Schneider et al. data do not show a consistent relationship between body size and head CG location, so a constant offset from tragion in head coordinates was used.)

The head orientation at each frame was expressed as the global transformation matrix associated with the head coordinate system. This orientation was interpreted as angles

based on sequential rotations around the local Y, X, and Z axes (the pitch-roll-yaw sequence).

Identifying Head Positions at the Event Start and Maximum Excursions

For each event, the data were extracted starting approximately one second prior to the onset of the event by visual inspection of the Kinect data. Head fitting was conducted for subsequent frames through the visually identified end of the event, typically about 3 seconds.

During data analysis, the vehicle acceleration data were used to define the start time (t-zero) for each trial. The data frame at which the absolute value of the acceleration on the primary axis (X for braking trials, Y for lane-change and turn-and-brake trials) first exceeded 0.2 g was identified. The acceleration gradient between this frame and the preceding frame was used to estimate the t-zero frame. For example, if the delta between the two frames was 0.1 g, the t-zero frame was identified as two frames prior to the first frame exceeding 0.2 g. The IMU and excursion data were time-shifted based on these calculations. Head excursion data were zeroed by subtracting off the head location at t-zero.

Test Conditions

Participants experienced four discrete vehicle maneuvers during a drive on the Mcity track. Events were experienced in the following sequence for all participants:

1. Braking abruptly while traveling straight (B1);
2. Turning sharply on a skid pad followed by abrupt braking (T1);
3. Braking abruptly on a surface street (B2); and
4. Quick lane-change to the right (L1).

For all events, prior to starting the maneuver, the participant was asked to answer a question from a questionnaire taped to the lap. The questions were administered as part of an effort to obfuscate the primary purpose of the study; the results were not analyzed. After each event, the vehicle stopped and an investigator explained that the maneuver was a simulation of an automated crash avoidance system and asked the participant to compare the severity of maneuver to similar maneuvers they have experienced. Leading into each event the investigator had engaged the cruise control to maintain the desired initial speed. Figure 31 shows the route on a map of the Mcity test facility, indicating the locations and sequence of the events, including the administration of the questionnaire. Figures 32-35 show locations of the specific maneuvers and typical linear acceleration traces.

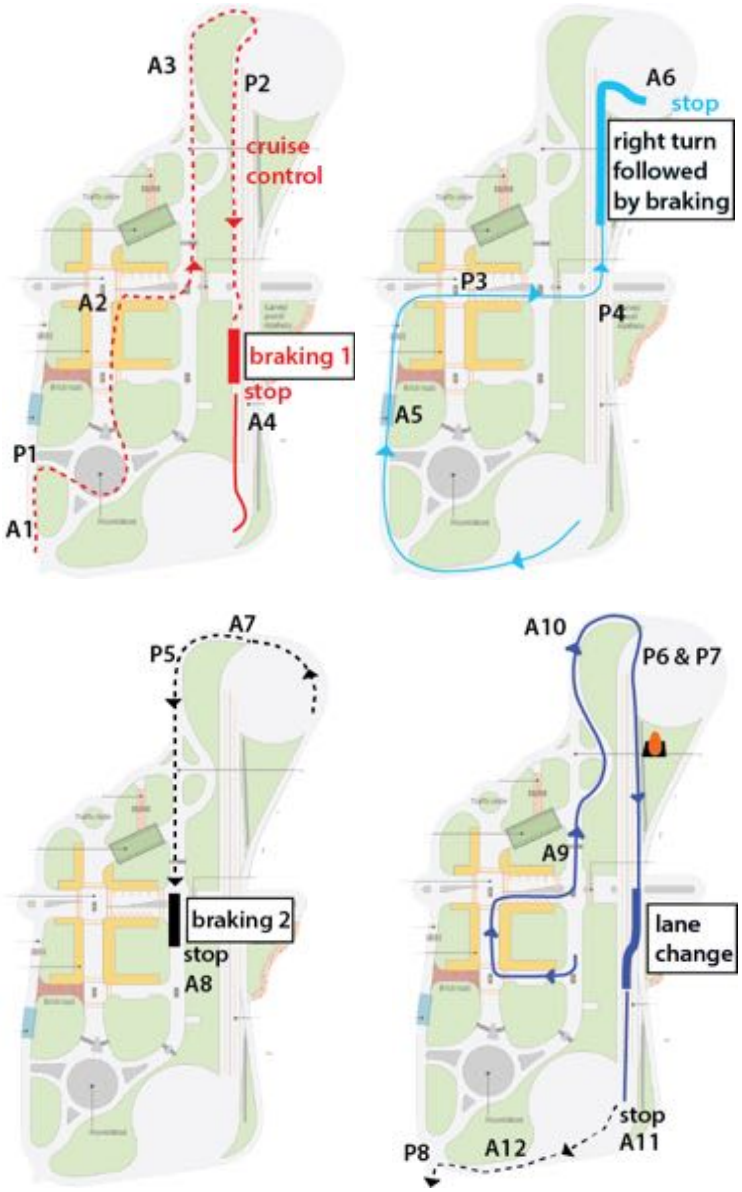

Figure 31. The location of events on a map of the Mcity test facility. Participants answered questions at specified locations: P = presented on the paper taped to their laps and A = asked aloud by the investigator.

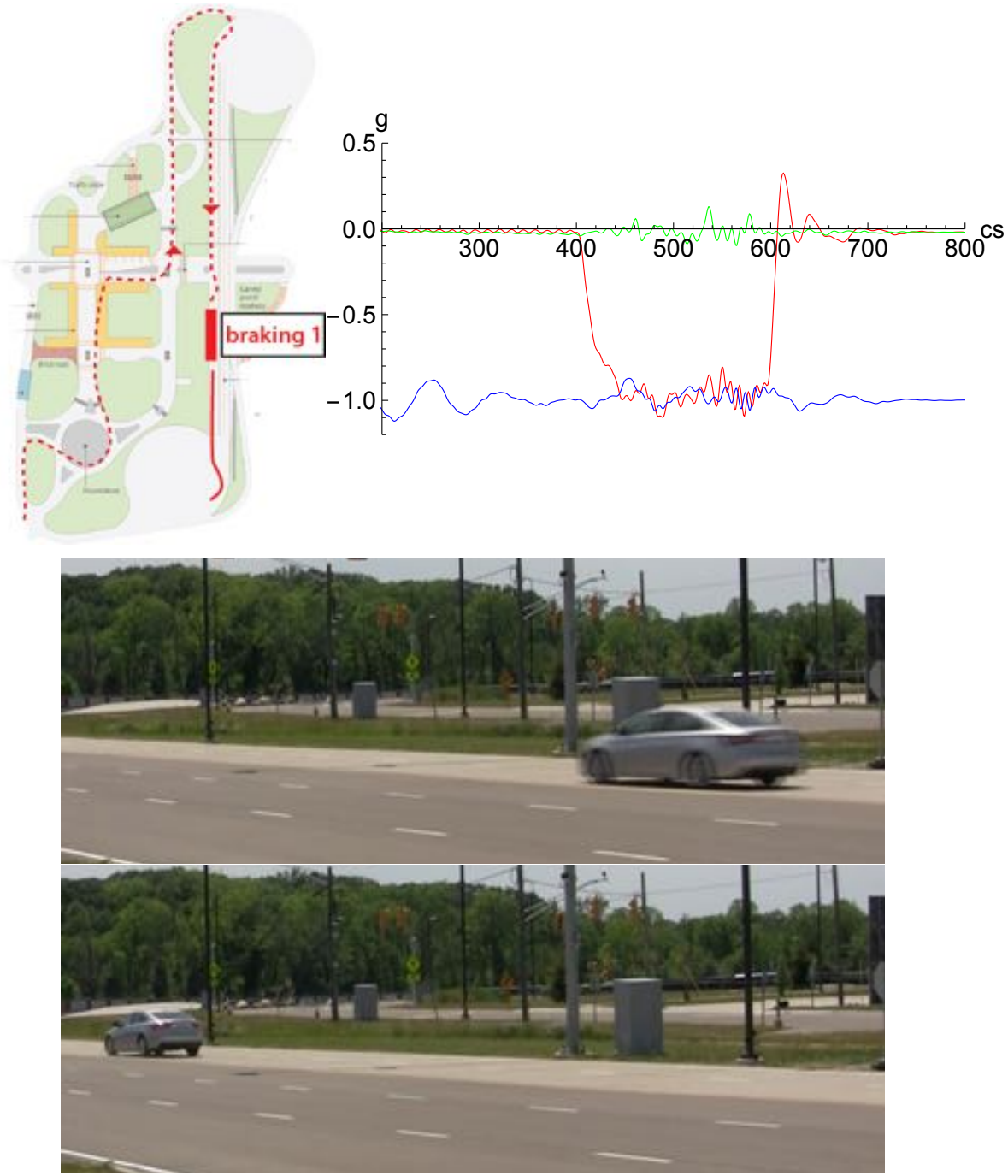

Figure 32. First braking maneuver. A typical acceleration trace is shown; (red, green, blue) = (x, y, z)

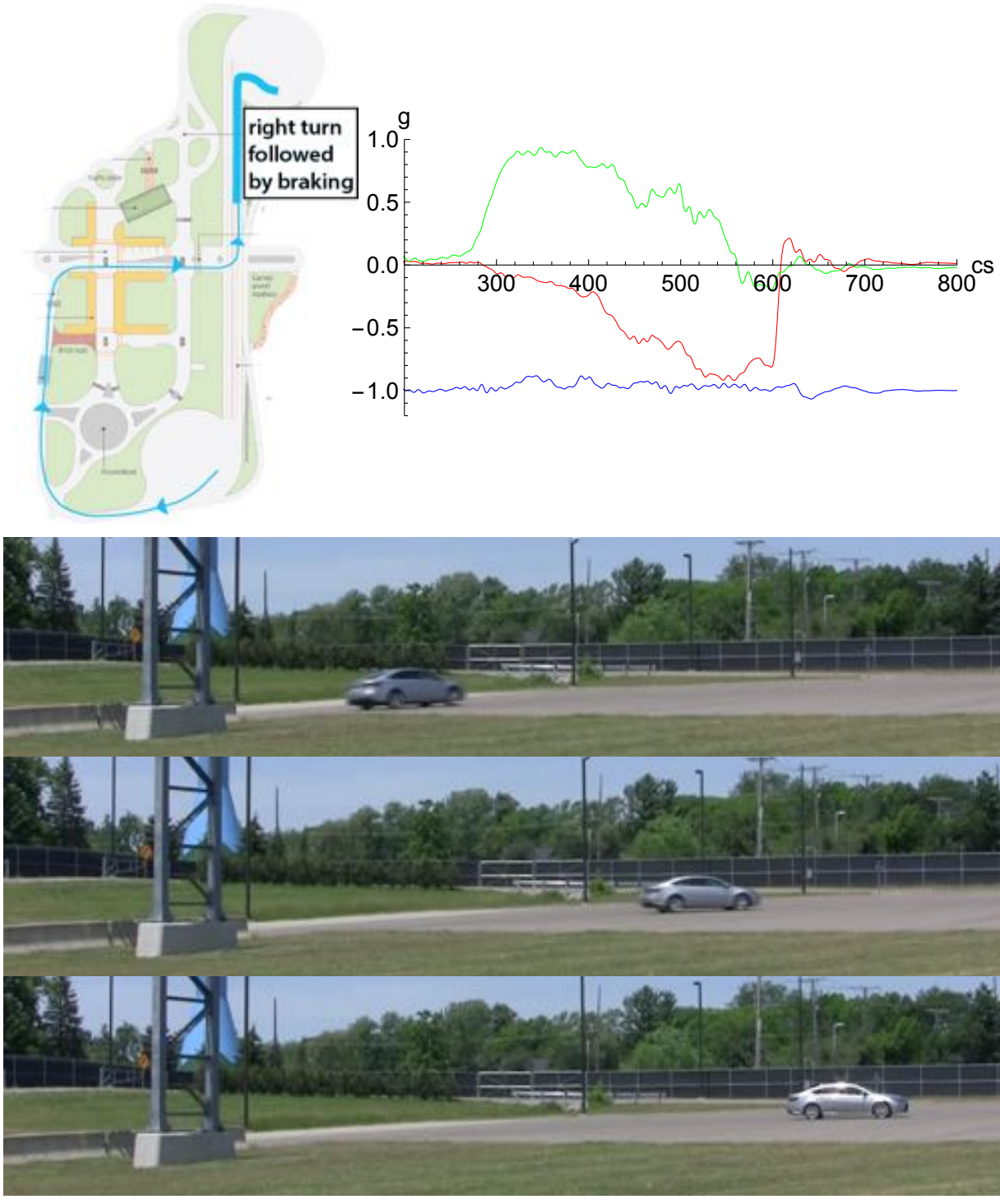

Figure 33. Turn and brake maneuver. A typical acceleration trace is shown: (red, green, blue) = (x, y, z)

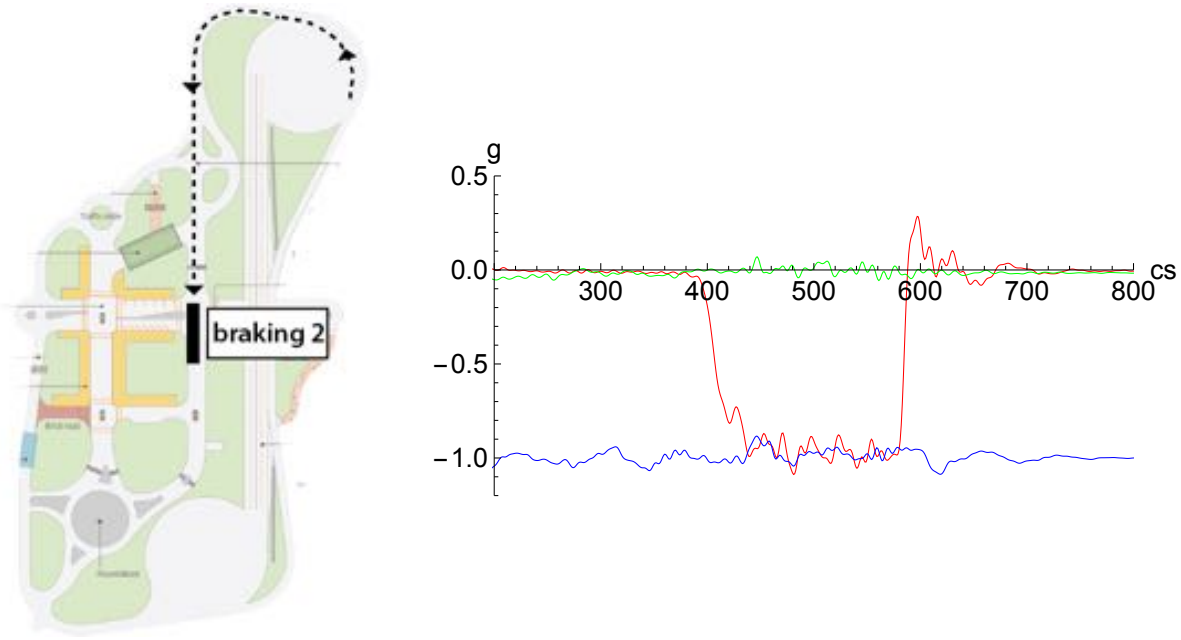

Figure 34. The second braking maneuver. A typical acceleration trace is shown: (red, green, blue) = (x, y, z)

Figure 35. The lane change maneuver; A typical acceleration trace is shown (red, green, blue) = (x, y, z)

RESULTS

Vehicle Acceleration Profiles

Data from the IMU showed that the acceleration profiles were consistent across trials. Figure 36a shows an overlay of longitudinal (X) acceleration from 20 braking trials. The acceleration typically reached -1 g after about 650 ms, with a total deceleration interval of about 2 s. Rebound typically reached about 0.3 g with a duration of about 0.2 s. Figure 36b shows lateral (Y) acceleration for 20 lane-change trials. Lateral acceleration in these trials typically peaked around 0.7 g with a pulse duration of about 1.2 seconds. The turn-and-brake trials produced lateral accelerations peaking at about 0.7 g approximately 700 ms into the event (Figure 36c). Longitudinal accelerations increased through the event, peaking around -1 g at about 2 s. The total event duration was typically 3 s. No relationship was found between the vehicle acceleration and head excursions for any of the events.

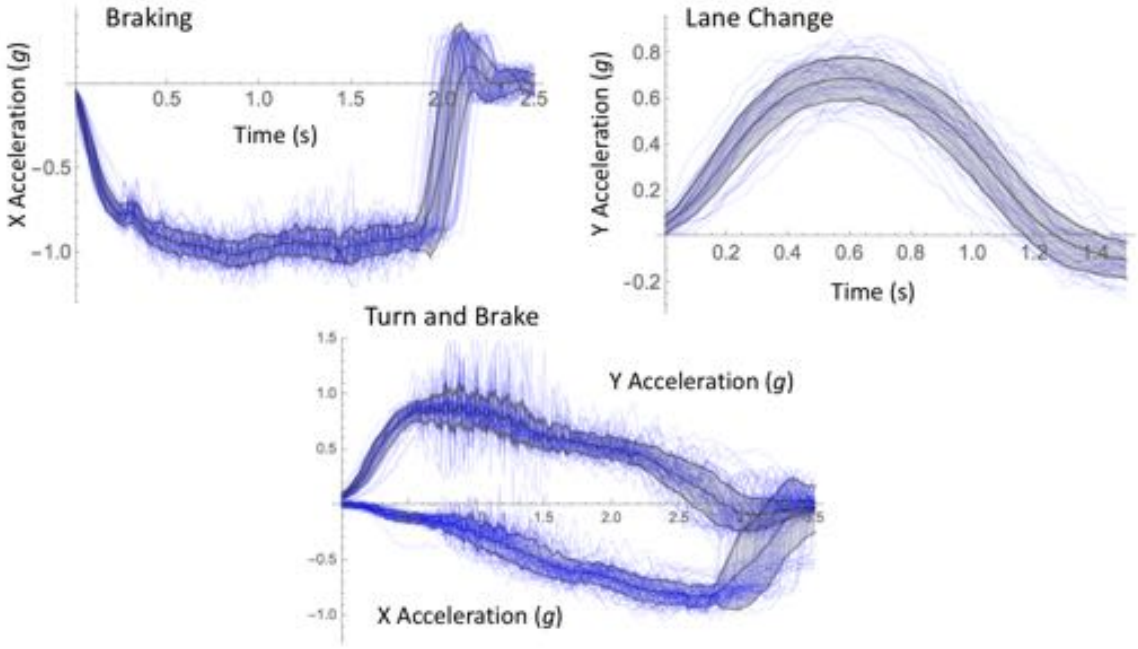

Figure 36. Overlay of longitudinal vehicle acceleration (g, s) from braking, lane-change, and turn-and-brake trials. Corridors are mean ± sd.

Qualitative Review of Passenger Reactions and Kinematics

Figure 37 shows images from three participants at the time of peak head excursion. In braking trials, most participants "rode" the belt, which locked early in the event. In lane-change and turn-and-brake trials, contact between the participant's arm and the center console appeared to limit inboard torso movement. Participants were readily able to

control their head position and orientation, and most maintained near-neutral head orientation. By design, in most trials the participants were looking down at the questionnaire taped to their thighs at the start of the event. Most looked up and remained looking up through the duration of the event, but others did not look up or looked up briefly and then looked back down at the paper.

Most of the participants exhibited visible surprise during the first braking event. Some reacted vocally, others by changes in facial expression, and several reacted by reaching out toward the door in an attempt to brace themselves. Reactions to subsequent events were more muted, but some participants continued to demonstrate surprised reactions to all events.

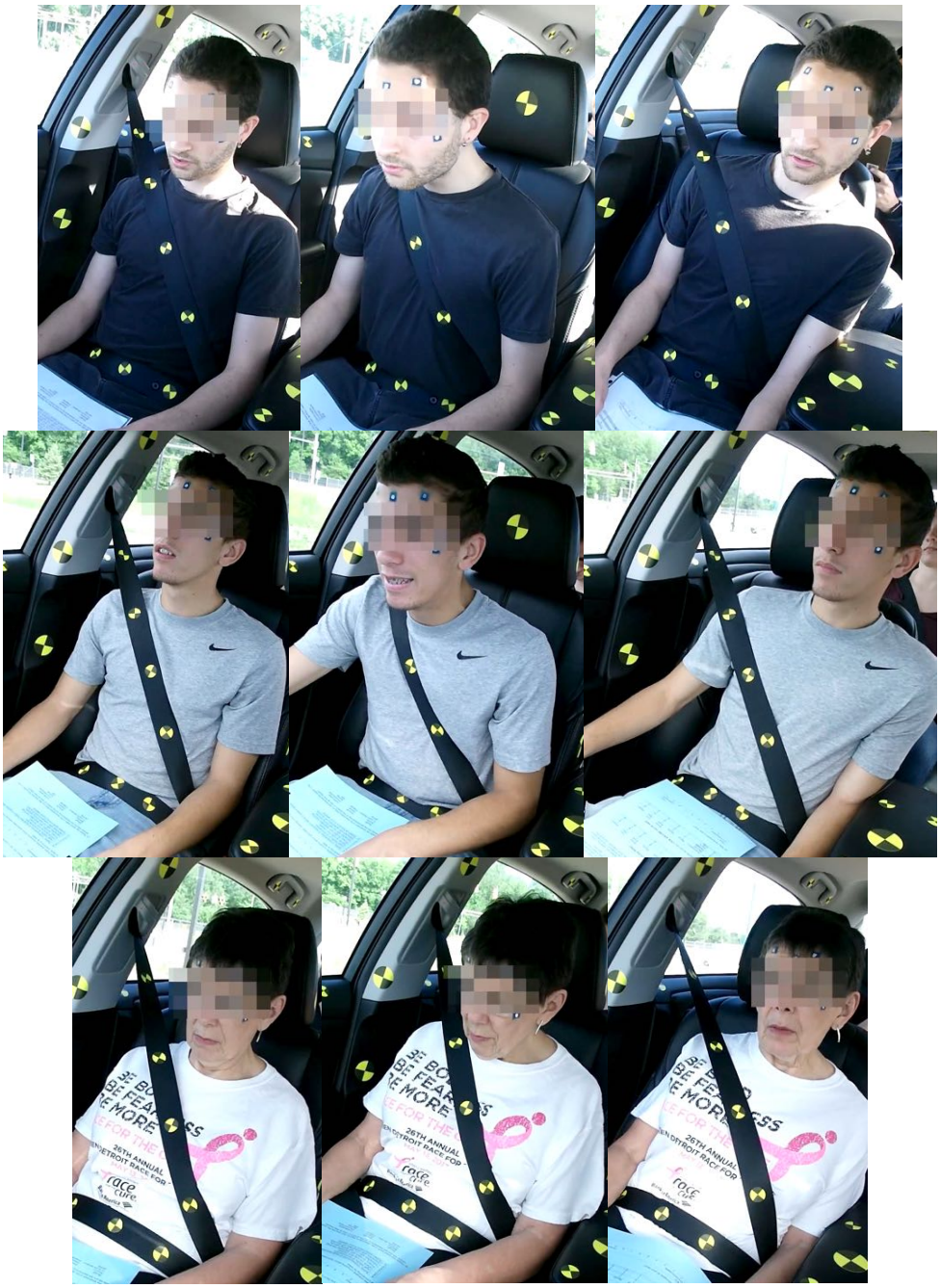

Figure 37. Sample images from starting (left) and maximum excursion frames for braking (center) and lane-change (right) events.

Head Excursions During Braking Events

Figure 38 shows the distribution of starting and maximum-forward head excursions in side and top view. The mean forward excursion is slightly larger than the range of initial fore-aft head positions relative to the seat. The range of fore-aft head locations is larger at the point of maximum excursion, and the distributions overlap only slightly. Overall, the

range of fore-aft head positions with respect to the seat H-point is more than twice as large when considering the initial and maximum-forward positions together.

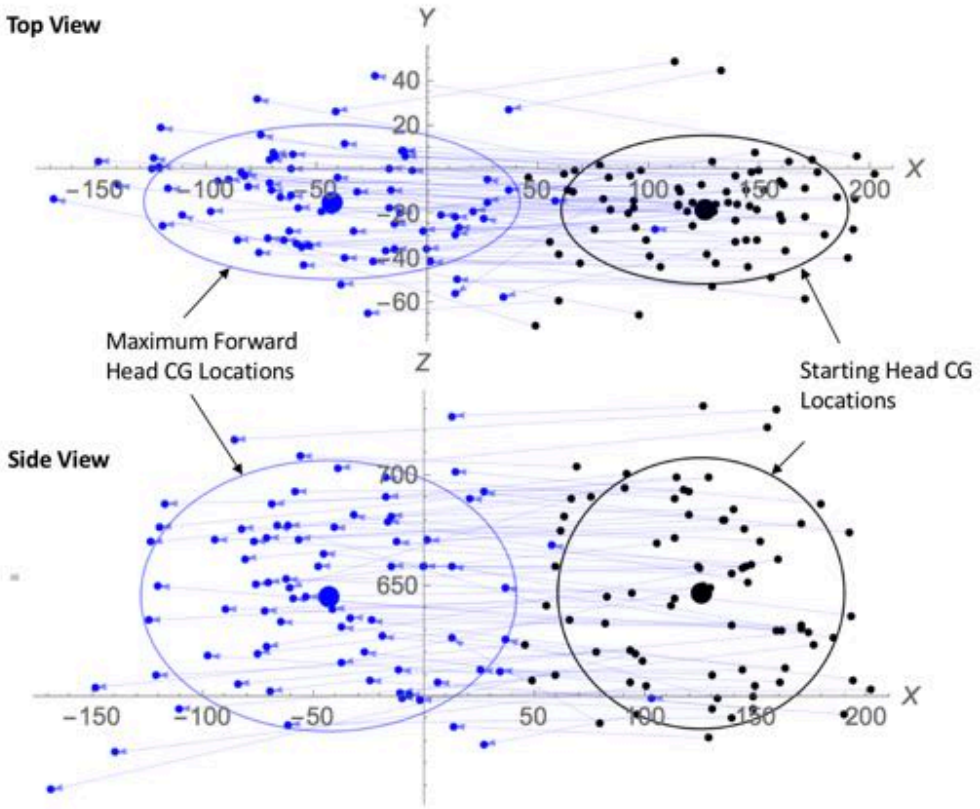

Figure 38. Top and side views of head CG locations in the **first braking** event. Arrows connect locations at the start of the trial and maximum forward excursion. Large dots are condition means and the ellipses are ±1.64 SD on each axis. The origin is the SAE J826 H-point, which remained fixed with respect to the vehicle for all subjects.

Figure 39 shows X-axis head excursion over time relative to the starting position in the first and second braking events. Considerable variability in the peak excursion is noted. Most participants' heads moved forward relative to the vehicle for about 0.4 s and then remained in approximately the same position for the duration of the event. Figure 39 shows corridors constructed as the mean ± 1 SD. (Note that the width of the corridor at the end of the event is due primarily to differences in the event duration rather than differences in participant behavior.)

In the first braking event, the mean (and standard deviation) of forward head excursion between 0.5 and 1.5 s was -135 (62) mm. The standard deviation was 46% of the mean. In the second braking event, the mean (sd) were -115 (58) mm; the standard deviation was 50% of the mean.

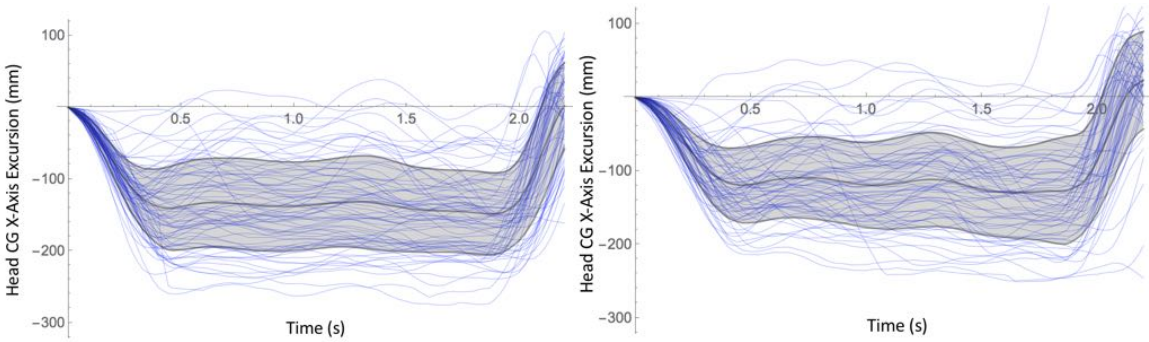

Figure 39. Forward (x-axis) head CG excursions in the first (left) and second (right) braking events. Corridors are mean ± SD.

Figure 40 shows a histogram of the mean values across participants in the interval between 0.5 and 1.5 s. These mean excursions are approximately normally distributed for the first event but are distributed in a more irregular pattern for the second. Data from both braking events were available for 68 participants. The mean forward excursion in the first braking exposure was larger than in the second for 49 (72%) of these participants. The difference in excursion between the trials was significantly different from zero using a paired *t*-test ($p<0.01$).

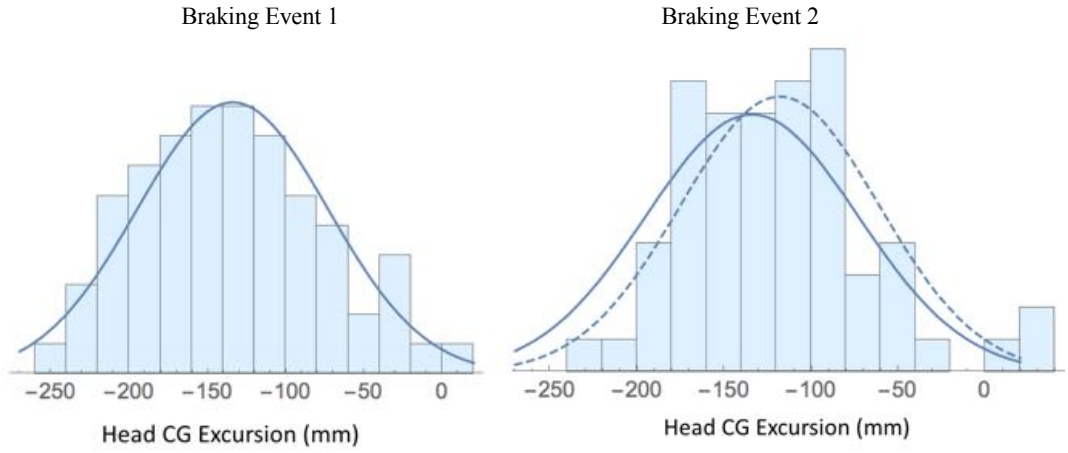

Figure 40. Distribution across participants of **mean** fore-aft head CG excursion between 0.5 and 1.5 s in first braking event (left) and second braking event (right). The normal approximation curve is shown for the first event (solid line). For the second event, the normal approximation curve is shown (dashed line) along with the normal approximation for the first event (solid line).

As expected, the maximum head CG excursions were somewhat larger than the mean excursions. Figure 41 shows cumulative distributions of the maximum fore-aft head CG excursions in the two braking events. The median maximum excursion was -166 mm for the first braking event and -148 mm for the second. Figure 42 shows a cross plot of maximum forward excursions in the two braking trials. The correlation was 0.73, indicating that participants who had larger excursions in the first trial tended to have larger excursions in the second.

In these trials, the maximum excursion in the first braking event was larger than in the second braking event for 47 (69%) of the participants. The difference in maximum excursion between the two trials was significantly different ($p<0.01$) using a non-parametric signed rank test.

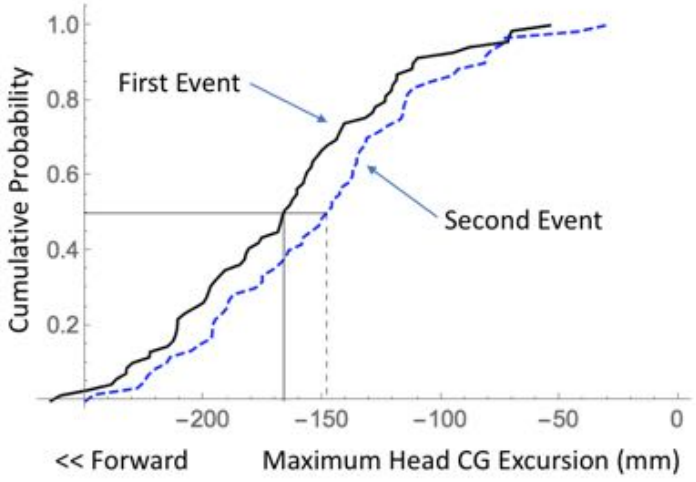

Figure 41. Cumulative distribution of maximum fore-aft head CG excursion in the two braking events.

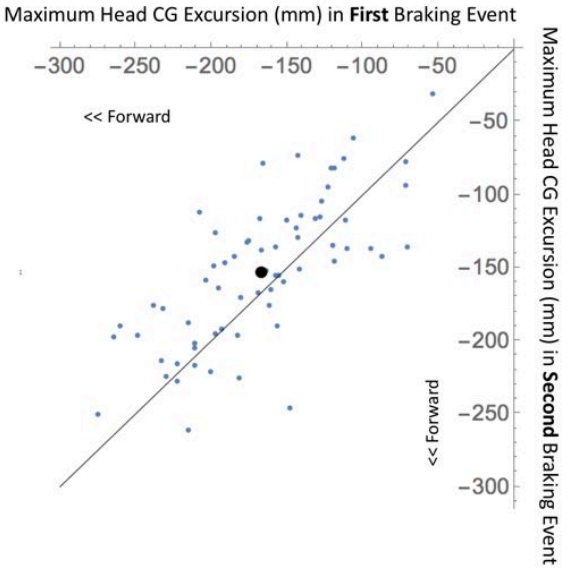

Figure 42. Cross plot of maximum x-axis head CG excursion in the first and second braking trials. The large dot shows the mean. Pearson $r = 0.73$. Line is 1:1.

Figure 43 shows plots of the mean and maximum x-axis excursions versus age, BMI, and stature for both braking events. The plots demonstrate that the variance is large relative to the effects of these covariates. The plots also show that the responses of male and female participants do not differ importantly.

Regression analyses were conducted to assess the influence of participant characteristics on excursions. Potential predictors included stature, BMI, erect sitting height, gender, and

age. Two-way interactions between trial (B1 vs. B2) and these covariates were also considered. For both the mean excursion (between 0.5 and 1.5 s) and the maximum excursion, only BMI and age were significant predictors ($p<0.01$), along with trial (B1 vs. B2). No two-way interactions with trial were significant. In all cases the adjusted R^2 value for prediction of the mean excursion was 0.17; for the maximum excursion R^2_{adj} was 0.25.

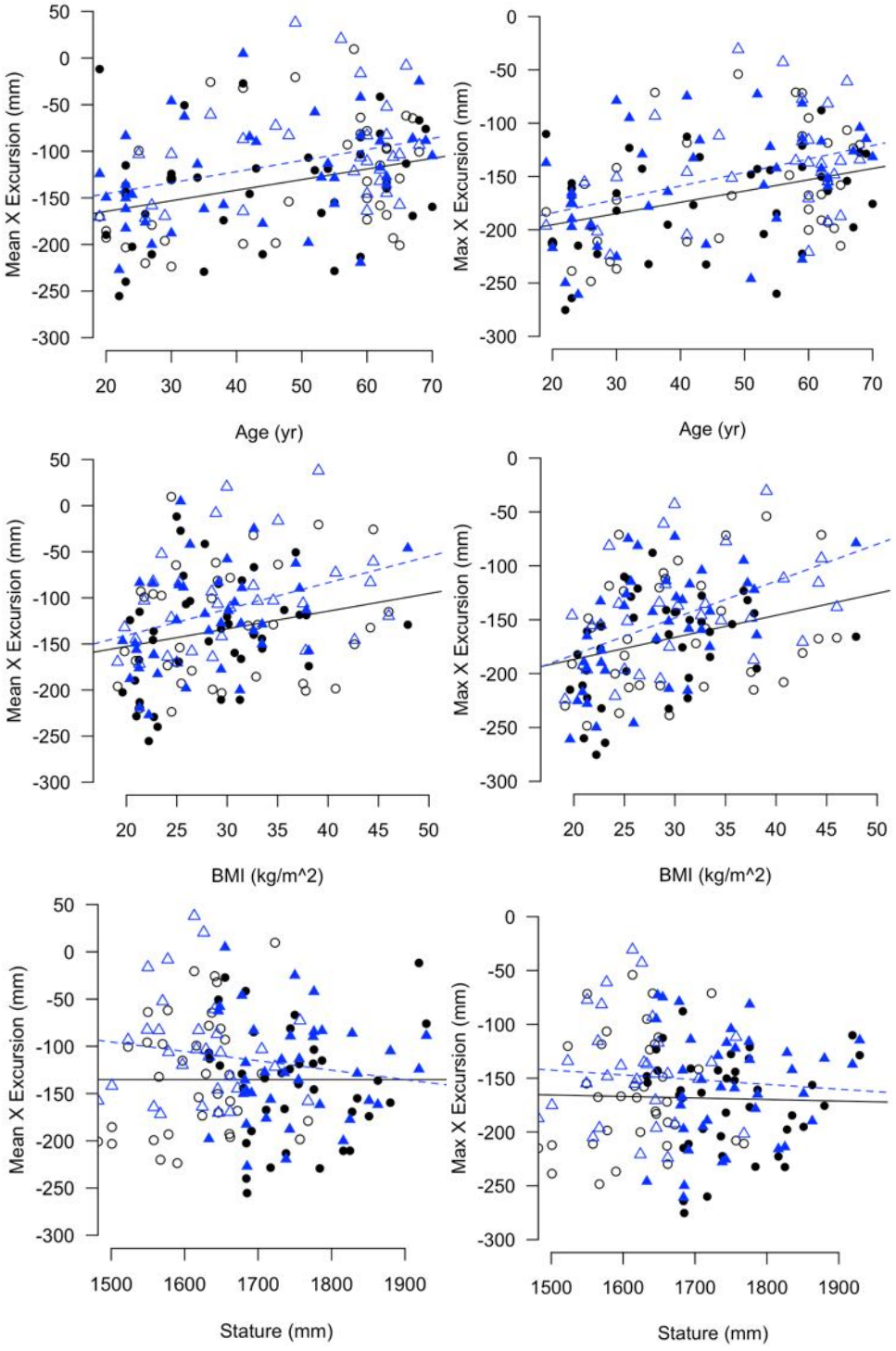

Figure 43. Effects of age and BMI on mean over the interval from 0.5 to 1.5 seconds (left) and maximum (right) forward excursion in braking trials. The first braking event is shown as circles and a solid regression line; the second event is triangles and a dashed line. Data from male and female participants are shown as filled and open symbols, respectively.

Head Excursions During Lane-Change Events

For lane-change events, the primary metric of interest is the inboard (y-axis) head excursion. Figure 44 shows the head CG locations at the start of the trials and at the maximum-inboard excursion. The mean head CG location started about 20 mm inboard of the seat centerline and ended about 140 mm inboard.

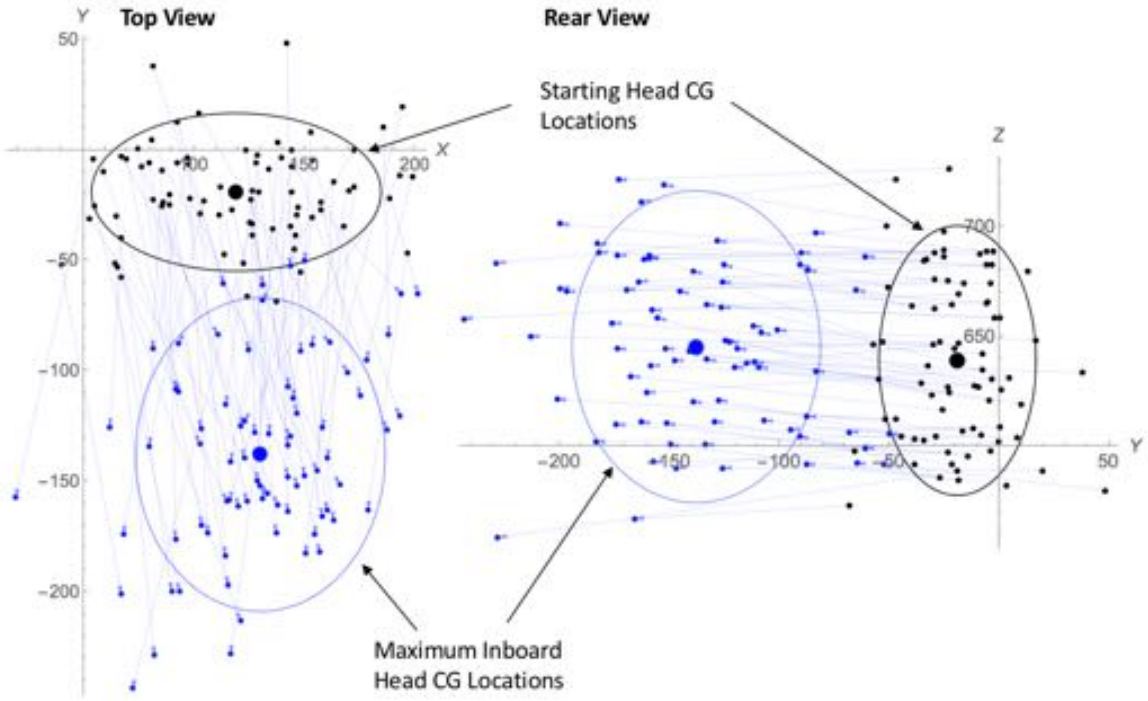

Figure 44. Top and rear views of head CG locations in the **lane-change** event. Arrows connect locations at the start of the trial and maximum forward excursion. Large dots are condition means and the ellipses are ±1.64 SD on each axis. The origin is the SAE J826 H-point, which remained fixed with respect to the vehicle for all subjects.

Figure 45 shows trajectories relative to the starting position along with mean±sd corridors. The excursion trajectories varied widely, though all showed an inward movement that lasted at least one second. In the middle of the event, between 0.4 and 0.9 seconds, the mean (sd) lateral excursion was -107 (40) mm. The standard deviation was 28% of the mean value. The mean maximum excursion was -118 (40) mm. Figure 47 shows histograms of the distribution of responses for the mean and maximum inboard excursion. The data are approximately normally distributed.

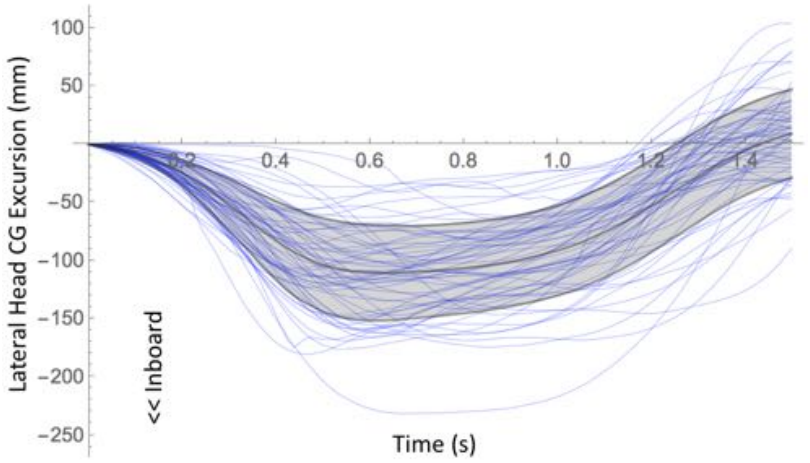

Figure 45. Inboard head excursions during lane-change trials. Corridor is mean±sd.

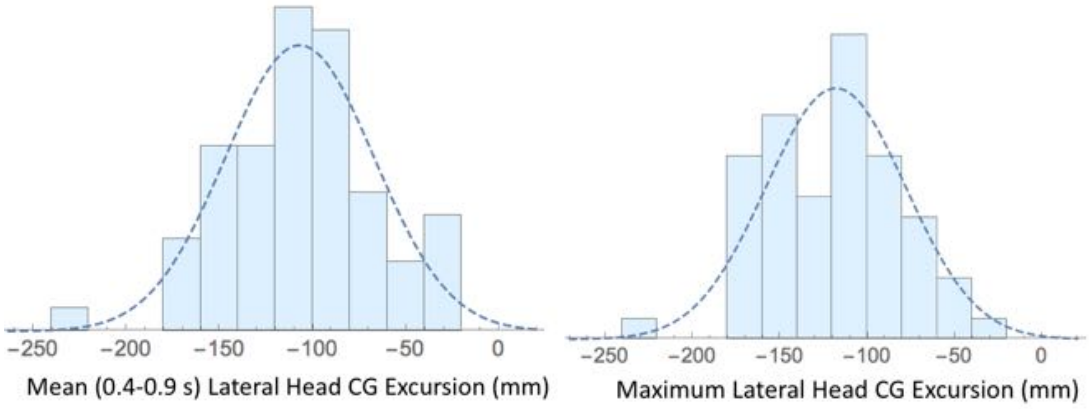

Figure 46. Distributions of lateral head excursion and approximating normal distributions.

Among potential predictors of both maximum and mean head excursion, only stature and erect sitting height were significant ($p<0.05$), but either variable accounted for less than 5% of the variance. Figure 47 shows the association with stature. On average, taller participants had slightly larger inboard excursions.

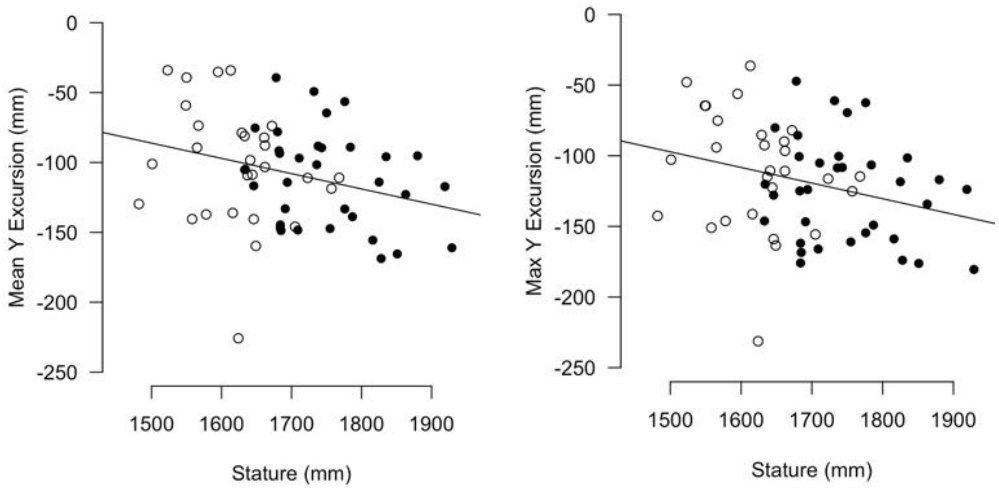

Figure 47. Association between stature and mean (left) and maximum (right) lateral head excursion in lane-change trials (negative = inboard). Data from male and female participants are shown as filled and open symbols, respectively.

Head Excursions During Turn-And-Brake Events

Head CG excursions during the turn-and-brake events were more variable than during the braking and lane-change events. Figure 48 shows the starting head CG locations along with the locations at the most-inboard and most-forward excursions. The distribution of inboard positions is similar to the lane-change trials (Figure 44), but the distribution of head locations at the point of maximum forward excursion is much larger, demonstrating a wide range of responses.

Figure 49 shows excursions on the X and Y axes versus time. Most participants moved their heads rearward as the turn began, in part by neck extension, regaining their initial fore-aft position after an average of 1.5 s in to the event. Most participants ended up with their heads forward of the initial position. The mean forward head displacement peaked after 2.8 seconds at –60 (40) mm. The lateral excursion early in the event was similar to the lane change. The mean inboard head movement peaked after 0.6 seconds at -131 (35) mm. As the braking acceleration increased, the head swung back toward the occupant midline, with a mean value of -30 mm at the time of peak mean forward excursion (2.8 s). A regression analysis found that the lateral excursion at 0.6 s was significantly related to stature ($p<0.01$), although it accounted for only about 9% of variance. The fore-aft excursion at 2.8 s was not significantly related to any participant covariates.

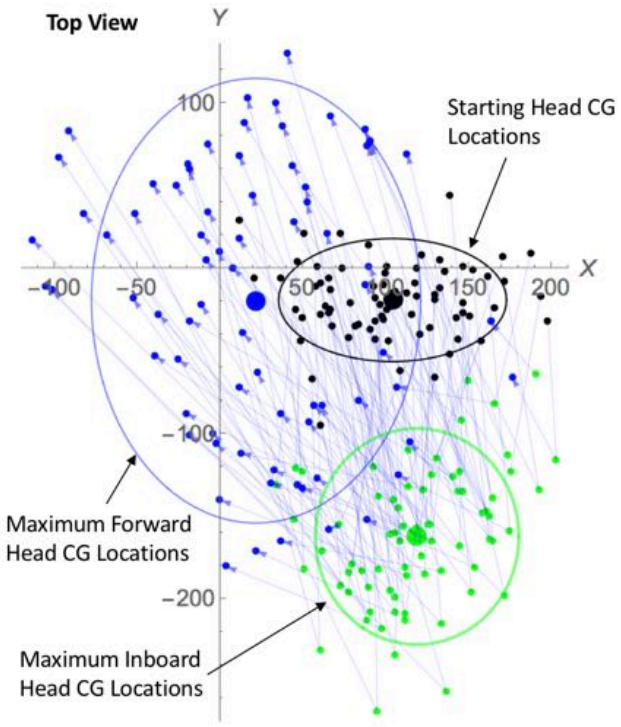

Figure 48. Top view of head CG locations in the **turn-and-brake** event. Arrows connect locations at the start of the trial, maximum inboard excursion, and maximum forward excursion. Large dots are condition means and the ellipses are ±1.64 SD on each axis. The origin is the SAE J826 H-point, which remained fixed with respect to the vehicle for all subjects.

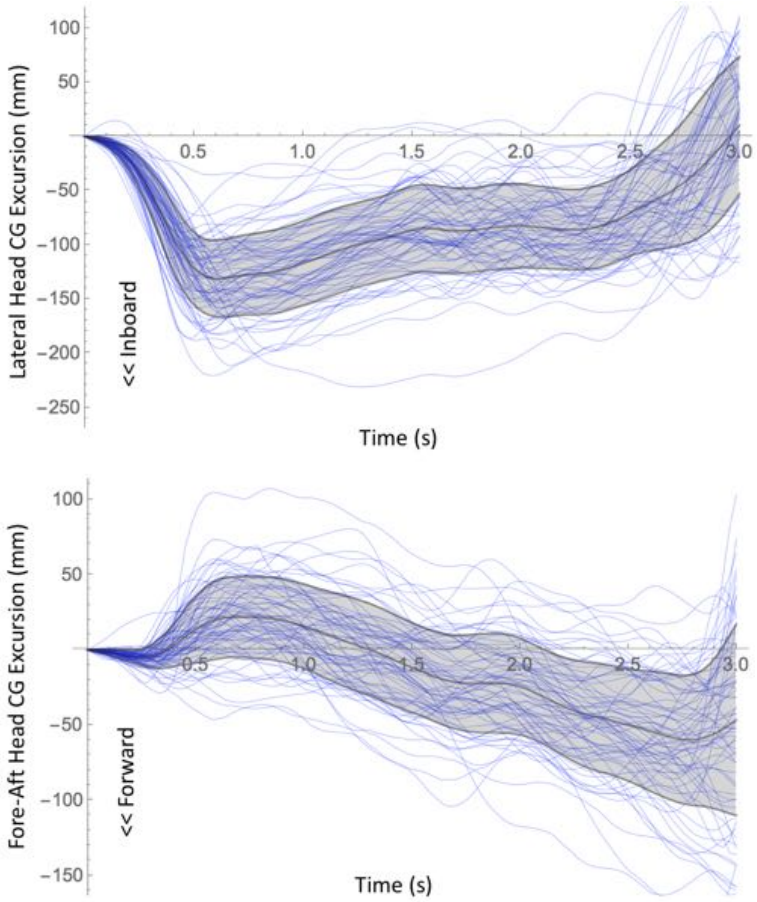

Figure 49. Lateral (top) and fore-aft (bottom) head CG excursions during turn-and-brake events. Corridors are mean±sd.

Head Angle Trajectories During Events

Head orientations typically remained within 15 degrees of the starting orientation. Most head movement was around the lateral axis (pitch), followed by rotation around the fore-aft axis (roll). By design, the participants were usually looking down at the questionnaire (negative pitch) at the start of the event. Some rotated their heads "up" during the event; some rotated back down to view the paper; and some kept their heads pitched forward the whole time.

Figure 50 shows absolute and relative (delta) corridors for pitch during braking events and roll during lane-change events. On average, participant's heads pitched forward about 10 degrees during braking events and rolled inboard about 4 degrees. However, the variance across individuals is so large that these values have little meaning. Participants were approximately as likely to increase head pitch as to decrease it. Overall, participants typically maintained their heads within 20 degrees of the initial global orientation during the events or engaged in voluntary motions. Rearward pitch change was as common as

forward pitch change during braking, and only a small number of participants exhibited more than 10 degrees of inboard head roll during the lane change.

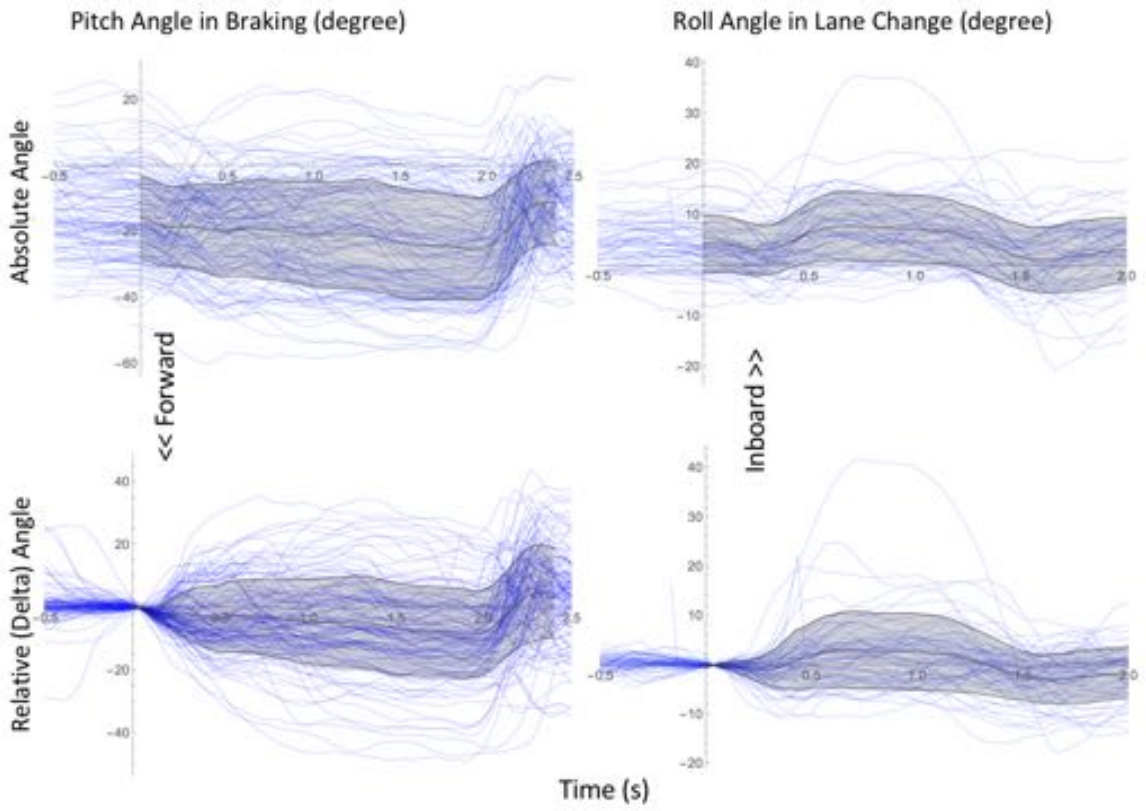

Figure 50. Mean±SD corridors overlaying individual angle trajectories for pitch (left) and roll (right). The plots at the top are absolute angles; the bottom plots are delta angles relative to the start of the event. Higher pitch is associated with neck extension ("looking up"); Higher roll is associated with the head tilting inboard.

Functional Analysis of Excursions

The preceding analyses have summarized time-series data as scalar values or aggregated time-aligned data to generate corridors without consideration of passenger characteristics. The effects of passenger characteristics were assessed using scalar outcome measures, such as mean or maximum excursions. Functional analysis considers each time-series or spatial curve as an observation and allows visualization and prediction of the effects of passenger characteristics on trajectories.

Applications of these methods to kinematics were pioneered in part at U-M. The basic methodology is described in Faraway and Reed (2007) and developed further in Samuels et al. (2015) and Sun et al. (2016). Measured trajectories are parameterized using basis splines (B-splines) that reduce the number of variables used to describe the trajectories and provide smoothing. A principal component analysis is applied to further reduce the complexity of the model. Typically, three to five principal components can account for 90% or more of the variance in kinematic data. Regression analysis is conducted to

predict principal component scores as a function of test conditions and participant descriptors such as stature and body weight. This methodology allows the typical behavior expected for a particular person (say, a 65-year-old woman with a stature of 1550 mm and BMI of 25 kg/m^2) to be predicted.

These methods can be further applied to compute corridors around these individualized predictions. This approach has strong advantages over typical approaches that rely on small subject cohorts. For example, Ólafsdóttir et al. (2013) presented separate corridors for men and women, with only 7 subjects in the female cohort. However, our data analysis with a much larger sample shows that male and female responses are not significantly different after taking into account body size. Hence, we can make predictions for individuals with the full range of adult stature using the combined dataset of both men and women.

Figure 51 shows head CG excursion corridors for braking generating using this functional modeling approach. As noted above, forward head excursion in braking is significantly related to age and BMI. The functional analysis demonstrated these effects by exercising the model with extreme values of these two variables. Corridors were generated by simulating 1000 trajectories for each passenger category based on the residual variance from the functional regression and the computing the standard deviation at each time point from these simulated trajectories.

Figure 52 shows analogous plots for inboard excursion in the lane-change event. The plots demonstrate that stature and BMI have larger effects than age. Note that because the predictors do not account of a large percentage of variance, the corridor widths are similar to those shown in Figure 45 for whole subject pool.

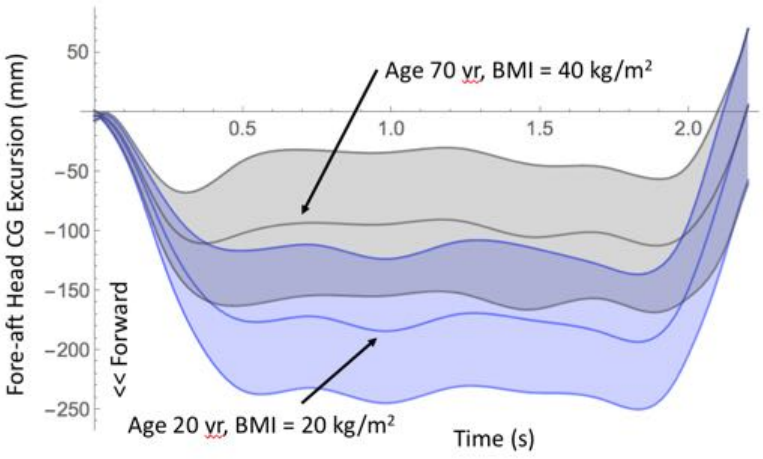

Figure 51. Corridors for **fore-aft head CG excursion in braking** generated by a functional modeling approach that takes into account passenger factors. The curves show the mean expected excursion ± 1 SD for two categories of passengers: older with high BMI, and younger with low BMI.

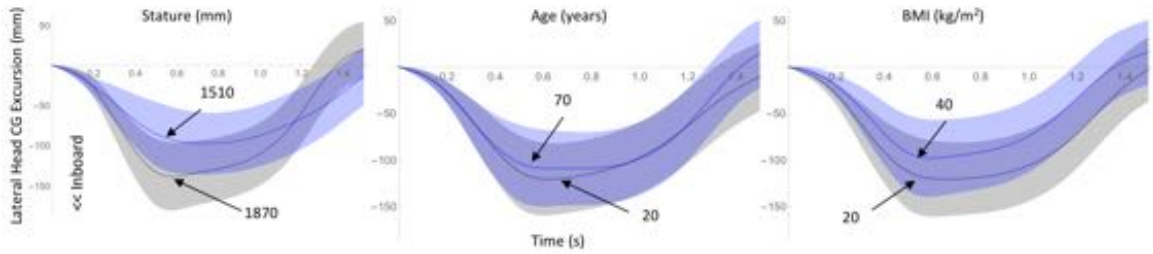

Figure 52. Corridors for **lateral head CG excursion in the lane-change maneuver** generated by a functional modeling approach that takes into account passenger factors. The curves show the mean expected excursion ± 1 SD for values of stature, age, and BMI that are approximately 5th and 95th percentiles in the dataset. In each plot, the other two variables are held at median values.

Figure 53 shows a similar analysis on spatial (Cartesian) head CG trajectories from the first braking trials. In this case, 2.2 seconds of data were zeroed to the starting head CG location and the functional analysis was conducted on all three coordinates over time. The mean predictions for four different combinations of age and BMI are shown. This analysis was conducted with 100 time-samples for each trajectory, and so the small movements during the plateau phase are captured. Smoother curves can be generated by fitting fewer splines to the data. The curves demonstrate the upward and inboard movement of the head as the torso pitches forward during the braking event. Only the group with the longest trajectories shows an appreciable downward motion near the maximum excursion indicative of substantial neck flexion (head pitching forward). These trajectories are associated with the youngest, thinnest passengers.

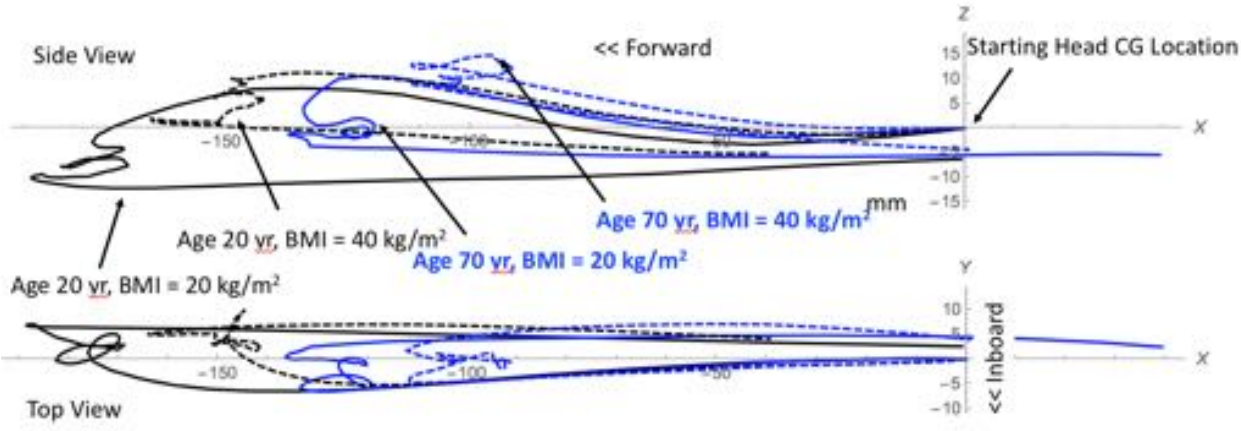

Figure 53. Predicted head CG trajectories in braking for two levels of stature and BMI. Predictions are generated by a functional analysis of head CG trajectories from 75 men and women with a wide range of age and stature.

Belt Fit Observations

A small number of obese participants were observed to experience belt fit that placed the shoulder portion of the belt high on the chest. Figure 54 shows two of these individuals. In both cases, the belt tended to ride up onto the neck during the braking events. The belt was observed to come off the shoulder during only one trial, a turn-and-brake event with a female participant with low BMI. Figure 55 shows an image during the maximum lateral excursion.

Figure 54. High belt routing on the torsos of two women with high BMI.

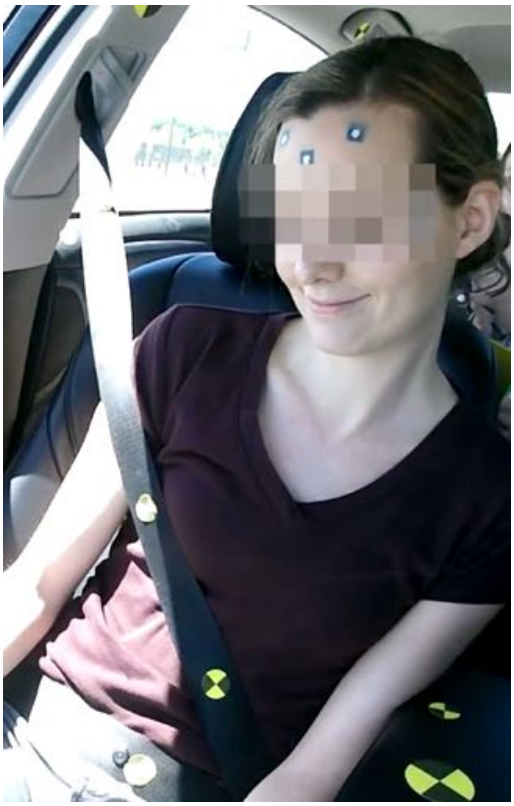

Figure 55. Belt off the shoulder of a participant during the turn-and-brake event. Note the elbow between the torso and console.

DISCUSSION

Overview

The most important findings from this study are:

- Head excursions during abrupt vehicle maneuvers are highly variable across individuals. This finding is broadly consistent with previous studies. Some individuals held themselves close to the initial posture, but all had some head movement associated with the events.

- Head excursions in vehicle maneuvers greatly expand the range of possible pre-crash head locations for passengers who are initially seated normally. In this study, the seat position was fixed, but a range of seat positions would normally be expected for passengers. The current findings indicate the associated distribution of head locations would be extended forward by about 200 mm under hard braking.

- Considerable residual variance in the trajectories remains after accounting for passenger characteristics. This is the first study with a large enough sample size to definitively investigate the effects of body dimensions and age; only modest effects were observed. Men and women have similar head excursions after accounting for body size.

- Head orientations are not strongly affected by the vehicle maneuvers – the head tends to move with the torso. Because the acceleration for these on-road maneuvers is limited to one g, the participants experience a level of force and moment on the neck that is common during normal activities, and the participants were able to move their necks freely during the event.

- Head excursions were significantly smaller in the second exposure, but the difference was small relative to the variance and hence not meaningful.

Comparisons with Prior Work

The findings from the current study are broadly consistent with prior studies. The most direct comparison is with Ólafsdóttir et al. (2013), who measured kinematics and muscle activity for 11 men and 9 women in the passenger seat of a sedan under maximal braking. The peak accelerations were close to 1.1 g, but otherwise the acceleration curves were similar to those obtained in the current testing. The head excursions were very similar to the current study, with a plateau of around -180 mm and a standard deviation in the plateau region of around 50 mm.

Carlsson and Davidsson (2011) measured passenger motions in braking events triggered during on-road driving. The typical peak acceleration was around 0.5 g. The forward head excursions for 17 men and women averaged 97 mm with a standard deviation of 47 mm. The higher excursions in the current are likely due to the higher accelerations, although the standard deviations are similar.

In a study of six women and 27 men, Kirchbichler et al. (2014) showed a small reduction in head excursions across two braking exposures, with values of -154(45) mm and -151(43) mm for the second, similar to the measurements in the current study. In a right-going lane-change maneuver, inboard maximum head excursions of -144 (39) mm were observed, compared with -118 (40) mm in the current study. Inboard head excursions were not significantly related to body size.

Implications

These findings have important consequences for simulating the effects of pre-crash maneuvers on alert but unaware passengers.

- The results do not support simple scaling of responses based on body size. Although BMI and stature had statistically significant relationships with forward and lateral head excursions, the functional relationships should be used rather than scaling.

- A modeling approach that maintains a fixed relationship between the torso, head, and neck will be well within the corridors generated from these data. That is, for the studied maneuvers, it is not necessary to produce complex neck kinematics.

- Because the kinematic responses vary so widely among individuals, muscle activation patterns will also be highly variable and not predictable from passenger characteristics. For active human body model simulations, the mean or typical response patterns will need to be modulated to produce the observed distribution of kinematic outcomes. Empirical data on muscle activity will be of greatest importance when the patterns of muscle activation influence injury patterns or risk in subsequent crash scenarios.

- The results support a stochastic view of the effects of pre-crash maneuvers. The findings indicate that passenger head locations are distributed over a fairly large range even when the occupants are alert, normally seated, and properly belted prior to the event. The resulting head locations overlap the normal seated head locations but also include locations further forward and further inward.

- Modeling of human responses to pre-crash maneuvers of the types studied here should aim to produce a large range of responses for all body sizes, rather than a single typical or average response for each body size in each maneuver. The mean responses across widely varying body sizes are essentially the same, but body size accounts for little of the population variance. Hence, simulations of all body sizes should aim to test restraint system performance across a wide range of postures.

Applications

These data have broad applicability to the design of safety systems. The data provide guidance on the range of pre-postures that are likely for adults in front passenger seats. Because about half of crashes are preceded by pre-crash maneuvers, the effects of such postures on crash outcomes should be investigated through crash simulations with ATDs and computational human models. The data indicate opportunities for pre-crash systems

to mitigate these posture changes, potentially improving restraint system performance during the crash.

The kinematics data also provide guidance for the development and application of active human body models that aim to simulate the pre-crash behavior of vehicle occupants. The current data augment previous datasets by including a much larger number of occupants with a wide range of body size and age. This study also introduced functional analysis methods that provide a means of establishing targets for specific human body model sizes.

Limitations and Future Work

The results are limited by the use of a single vehicle and seat. The seat design and the presence of the console may have limited lateral excursions. In particular, review of videos showed that nearly all participants' torsos were braced against the center console with their elbows and arms in the lane-change and turn-brake scenarios. A situation without a console, or with the console farther from the seat centerline, may have produced larger excursions in these trials. The location of the upper belt anchorage D-ring may also have influenced the results. Because the seat was placed full rearward, the D-ring was only slightly behind the shoulders of some participants. A more-rearward D-ring location relative to the shoulder may have resulted in greater restriction of excursion, since the belt force would be directed more rearward. Similarly, a seat-integrated retractor might reduce variance in the belt-to-shoulder relationship and reduce excursions.

The particular design of the retractor may have affected the forward excursions in braking. A design that locked more quickly may have reduced excursions. Previous research has shown that a motorized pre-pretensioner that removes belt slack can reduce forward excursions for passengers during hard braking (Ólafsdóttir et al. 2013) and may reduce lateral excursions as well (Bohmann et al. 2011).

The turn-and-brake scenario was hypothesized to yield higher forward excursions due to a shift in the shoulder belt relative to the torso during the lane change. However, the belt remained on the shoulder for nearly all participants, and as a consequence the forward movement during the turn-brake scenario was not greater than in the braking trials. Forward excursions were determined primarily by the belt webbing length at the time the retractor locked.

During braking, large changes in the backset between the head and head restraint were observed. During rebound, many participants' heads moved rapidly rearward and contacted the head restraint. These results suggest the possibility of highly variable kinematics in rear impacts that occur at different times during a braking event. Recent analyses of crash data have suggested that automatic emergency braking may increase rear-end struck crashes by 20%, increasing the importance of protection in these crashes (Cicchino 2017).

An automatic emergency braking system could produce a brake onset that differs from the manual activation used in this study. If the automated braking was more abrupt, greater forward excursion might occur before the passenger is able to react, but vehicle automation could also take into account passenger movements when determining an optimal response to a pre-crash situation (Kim et al. 2015). Similarly, more-rapid lateral motions could be triggered by vehicle automation, potentially resulting in greater excursions. However, the current results suggest that the variability would still be large relative to the mean excursions.

Longer-duration events of similar acceleration magnitude, for example braking from a higher speed, would probably have produced similar results, because the non-voluntary head excursions were essentially stable after less than one second. However, many other pre-crash vehicle motions are possible. This study considered only on-road, vehicle-induced accelerations. A vehicle that leaves the roadway can experience higher and more variable accelerations due to, for example, entering a ditch or furrowing through soft ground. In these cases, both planar and non-planar accelerations higher 1 g are possible could result in increased and more complex excursions.

Belt fit and posture in this study were optimal. A wider distribution of postures and belt fit would be expected with passengers in normal settings. Many of these alternatives, such as looser belt fit, heavy clothing under the belt, and leaning postures are likely to result in larger excursions. Differences in lower-extremity posture could also affect the results.

The study population was ambulatory and free of reported musculoskeletal injury or disability that would have affected their ability to participate. Some vehicle occupants may have less ability to control posture due to injury or disability.

Additional information is available in the data from the current study. In particular, torso motions and belt positions can be digitized in the 3D data obtained from the Kinect sensor. These data could be combined with the head motion data to obtain a more complete description of body movements. Qualitatively, the torso was observed to move as unit, sliding forward or sideways until restrained by the belt or the console. This movement did not appear to include sliding between the participant's clothing and the seat cushion; rather, lateral movement of the skeleton in the pelvis area was likely primarily internal. Little lumbar motion was observed, but only a few degrees of flexion or lateral bending would be sufficient to produce the observed upper-torso motions.

REFERENCES

Bohman, K., Stockman, I., Jakobsson, L., Osvalder, A-L., Bostrom, O., Arbogast, K.B. (2011). Kinematics and shoulder belt position of child rear seat passengers during vehicle maneuvers. *Annals of the Association for the Advancement of Automotive Medicine.* 55: 15–26.

Carlsson, S. and Davidsson, J. (2011). Volunteer occupant kinematics during driver initiated and autonomous braking when driving in real traffic environments. *IRCOBI.*

Chang CY, Rupp JD, Kikuchi N, Schneider LW (2009) Predicting the Effects of Muscle Activation on Knee, Thigh, and Hip Injuries in Frontal Crashes Using a Finite-Element Model with Muscle Forces from Subject Testing and Musculoskeletal Modeling. *Stapp Car Crash Journal* 53:291–328.

Cicchino, J.B. (2017) Effectiveness of forward collision warning and autonomous emergency braking systems in reducing front-to-rear crash rates. *Accident Analysis and Prevention*, 99:142-152.

Ejima, S., Zama, Y., Ono, K., Kaneoka, K., Shiina, I., Asada, H. (2009). Prediction of pre-impact occupant kinematic behavior based on the muscle activity during frontal collision. *ESV*.

Faraway, J.J. and Reed, M.P. (2007). Statistics for digital human modeling in ergonomics. *Technometrics*. 49:262-276.

Hault-Dubrullea, A., Robachea, F., Pacauxa, M-P, and Morvana, H. (2011). Determination of pre-impact occupant postures and analysis of consequences on injury outcome. Part I: A driving simulator study. *Accident Analysis and Prevention* 43: 66–74

Huber, P., Kirschbichler, S., Prüggler, A., and Steidl, T. (2015). Passenger kinematics in braking, lane change and oblique driving maneuvers. *IRCOBI.*

Iwamoto M, Nakahira Y, Kimpara H, Sugiyama T (2012) Development of a Human Body Finite Element Model with Multiple Muscles and their Controller for Estimating Occupant Motions and Impact Responses in Frontal Crash Situations. *Stapp Car Crash Journal* 56:231–268.

Kim, E-S., Min, D-H, Sung, S-M, and Lee, C-B. (2015). The AEB system with active and passive safety intergration for reducing occupants' injuries in high-velocity region. *Proc. ESV.*

Kirschbichler, S., Huber, P., Prüggler, A., Steidl, T., Sinz, W., Mayer, C., and D'Addetta, G.A. (2014). Factors influencing occupant kinematics during braking and lane change maneuvers in a passenger vehicle. *IRCOBI.*

Morris, R. and Cross, G. (2005). Improved understanding of passenger behavior during pre-impact events to aid smart restraint development. *ESV*.

Ólafsdóttir, J.M., Östh, J.K., Davidsson, J., Brolin, K.B. (2013). Passenger kinematics and muscle responses in autonomous braking events with standard and reversible pre-tensioned restraints. *IRCOBI.*

Östh J, Ólafsdóttir J M, Davidsson J, Brolin K, (2013). Driver kinematic and muscle responses in braking events with standard and reversible pre-tensioned restraints: Validation data for human models. *Stapp Car Crash Journal*, 57.

Östh J, Brolin K, Bråse D (2014a) A Human Body Model with Active Muscles for Simulation of Pre-Tensioned Restraints in Autonomous Braking Interventions. *Traffic Injury Prevention* 16(3):304–313.

Östh J, Brolin K, Carlsson S, Wismans J, Davidsson J (2012a) The Occupant Response to Autonomous Braking: A Modeling Approach that Accounts for Active Musculature. *Traffic Injury Prevention* 13(3):265–277.

Östh J, Brolin K, Happee R (2012b) Active Muscle Response using Feedback Control of a Finite Element Human Arm Model. *Computer Methods in Biomechanics and Biomedical Engineering* 15(4):347–361.

Östhmann, M. and Jakobsson, L. (2016). An Examination of Pre-crash Braking Influence on Occupant Crash Response using an Active Human Body Model. *Proc. IRCOBI.*

Park, B. K., Lumeng, J. C., Lumeng, C. N., Ebert, S. M., & Reed, M. P. (2015). Child body shape measurement using depth cameras and a statistical body shape model. *Ergonomics*, *58*(2), 301-309.

Park, B-K.D., Jones, M.L.H., Miller, C., Hallman, J., Sherony, R., and Reed, M.P. (2018). In-vehicle occupant head tracking using a low-cost depth camera. SAE Technical Paper 2018-01-1172. SAE International, Warrendale, PA.

Reed, M.P., Ebert, S.M., and Hallman, J.J. (2013). Effects of driver characteristics on seat belt fit. *Stapp Car Crash Journal*, 57:43-57.

Samuels, M.A., Reed, M.P., Arbogast, K.B., and Seacrist, T. (2015). Modeling spatial trajectories in dynamics testing using basis splines: application to tracking human volunteers in low-speed frontal impacts. *Computer Methods in Biomechanics and Biomedical Engineering.* 10.1080/10255842.2015.1091886

Stockman, I. (2016). Safety for Children in Cars – Focus on Three Point Seatbelts in Emergency Events. PhD Dissertation, Chalmers University.

Schneider, L.W., Robbins, D.H., Pflüg, M.A., and Snyder, R.G. (1983). Anthropometry of Motor Vehicle Occupants: Development of anthropometrically based design specifications for an advanced adult anthropomorphic dummy family, Volume 1. Final report DOT-HS-806-715. U.S. Department of Transportation, National Highway Traffic Safety Administration, Washington, DC.

Sun, W., Jin, J.H., Gayzik, F.S., Danelson, K.A., Bass, C.R., Zhang, J.Y., and Rupp, J.D. (2016). A method for developing biomechanical response corridors based on principal component analysis. *Journal of Biomechanics,* 49(14):3208-3215.

Appendix A
Participant Questionnaire – Paper

Automated Vehicles Questionnaire (please do not read ahead)

1) Rate the ease or difficulty of maintaining your posture through this turn

Very Difficult									Very Easy
1	2	3	4	5	6	7	8	9	10

2) Please say aloud each of the descriptions that you feel describe the quality of the vehicle ride you are experiencing on this stretch of road as they happen

Rough	Smooth	Comfortable
Bouncy	Uneven	Uncomfortable
Too much vibration	Irregular	Spongy
Jarring		Stiff

3) How interested would you be in purchasing an automated vehicle?

Not Interested									Very Interested
1	2	3	4	5	6	7	8	9	10

4) Rank these possible concerns about automated vehicles from most concerning to least concerning by letter

A	Safety consequences of equipment failure or system failure
B	Legal liability of drivers/owners
C	Vehicle security from hackers
D	Privacy (location and destination tracking)
E	Interaction with non-self driving vehicles
F	Interaction with pedestrians and bicyclists
G	System performance in poor weather

5) Please say aloud each of the descriptions that you feel describe the quality of the vehicle ride you are experiencing on this stretch of road as they happen

Rough	Smooth	Comfortable
Bouncy	Uneven	Uncomfortable
To much vibration	Irregular	Spongy
Jarring		Stiff

Manual driving: The human driver executes the driving task him/herself using the steering wheel and pedals.

Partially automated driving: The automated driving system takes over both speed and steering control on all roads. However, the system cannot handle all possible situations. Therefore, the driver shall permanently monitor the road and be prepared to take over control at any time.

Highly automated driving: The automated driving system takes over both speed and steering control on all roads. The driver is not required to permanently monitor the road. If automation cannot handle a situation it provides a take-over request, and the driver must take-over control with a time buffer of 7 seconds

Fully automated driving: The system takes over speed and steering control completely and permanently, on all roads and in all situations. The driver sets a destination via a touchscreen. The driver cannot drive manually, because the vehicle does not have a steering wheel.

6) How frequently would you **WATCH the ROAD**?

Question	Automation	Never	Rarely	Some-times	Very Often	Always
A	Manual	1	2	3	4	5
B	Partially	1	2	3	4	5
C	Highly	1	2	3	4	5
D	Fully	1	2	3	4	5

7) How frequently would you **LOOK AROUND (not at road)**?

Question	Automation	Never	Rarely	Some-times	Very Often	Always
E	Manual	1	2	3	4	5
F	Partially	1	2	3	4	5
G	Highly	1	2	3	4	5
H	Fully	1	2	3	4	5

8) How comfortable is your seat?

Very Uncomfortable									Very Comfortable
1	2	3	4	5	6	7	8	9	10

Appendix B
Participant Questionnaire -- Investigator Form and Oral Questions

Investigator:_____ Participant:_____

Course Questionnaire

Introduction

During this drive you will be asked a series of questions which you will answer aloud. Some of the questions will be on the piece of paper you are holding. If it is on the paper, I will give you the question number. You will read the question to yourself and then answer aloud. I will also ask you questions that are not on the paper. We may not ask you all of the questions in front of you. **Please do not read questions before being asked to.**

LOOP1

After entering Mcity: We are now going to start asking you questions.

Aloud 1: *After entering Mcity, with the vehicle stopped*

Is the level of engine noise you hear acceptable, yes or no? ___Y ___ N

Paper 1: *As you are entering the round-about*

Please read question number 1 and respond. _____

Aloud 2: *After stopping at the intersection*

Was that stop too abrupt or just right? ___Too Abrupt __Just Right

Aloud 3: *While going up the hill*

Was that acceleration too fast, too slow or just right?

____Too Fast ____Too Slow ____Just Right

Paper 2: *At the pause before braking event 1*

Please read question number 2 and respond.

Adjectives:_____

Aloud 4: *After braking event 1*

Some new cars have automatic braking that comes on when a frontal collision is likely. We used a manual braking event to simulate automated braking.

Was that braking event less severe than others you've experienced, more severe, or about the same? OK, we're going to go on with the drive now.

Response:

LOOP 2

Aloud 5: *While going under covered bridge*

Was that acceleration too fast, too slow or just right?

____Too Fast ____Too Slow ____Just Right

Paper 3: *While going through town/ going up hill*

Please read question number 3 and respond. _____

Paper 4: *As the driver sets the cruise control for the turn/braking*

Please read question number 4 and respond.

Order:_____

Aloud 6: *After for turn/braking*

Some new cars have an "avoidance assistant" system that intervenes in steering to help the driver avoid an obstacle. We used a manual turning to simulate this system.

Was the turn less severe than others you've experienced, more severe, or about the same? OK, we're going to go on with the drive now.

Response:

Investigator:_____ Participant:_____

LOOP 3

Aloud 7: *After the curve at the top of the hill*

Was that turn too fast, too slow, or just right?

___Too fast ___Too Slow ___Just Right

Paper 5: *At the pause before event breaking event 2*

Please read question number 5 and respond.

Adjectives:_____

Aloud 8: *After turn/braking and lane change*

This was another example of a simulated automatic braking.
Was the turn less severe than others you've experienced, more severe, or about the same?
Response:

Please flip the paper you have on your lap to the back-side, and once again, please do not read ahead.

LOOP 4

Aloud 9: *After turning to go up the hill*

On this next stretch of road please let us know each time you feel a bump in the road. *(make a mark each time they indicate a bump)*

Aloud 10: *At pause before starting lane change*

As a passenger, do you think that the windshield in front of you allows you to see enough of your surroundings, yes or no? ___Y ___ N

At pause before starting lane change: please review the definitions of vehicle automation.

Paper 6 & 7: *Before lane change*

Please read questions number 6 and 7 and respond with the question letter and the number of your ranking.

A___	E___
B___	F___
C___	G___
D___	H___

Aloud 11: *After lane change*

This was another simulation of obstacle avoidance. Was the lane change less abrupt than others you've experienced, more abrupt, or about the same?
Response:

As Leaving (waiting for gate)

Aloud 12: *As leaving Mcity*

Is the height of your seat above the vehicle floor too low, too high, or just right?
___Too Low ___Too High ___Just Right

Paper 8: *As leaving Mcity*

Please read question number 8 and respond. _____

Appendix C
Participant Anthropometry

Subject	Gender	Age (yr)	Stature (mm)	Weight (kg)	BMI (kg/m^2)	Sitting Height (mm)	SH/S*
TD001	MALE	24	1684	55.7	19.6	886	0.526
TD002	MALE	38	1851	130.5	38.1	984	0.532
TD003	MALE	23	1684	65.5	23.1	903	0.536
TD004	MALE	63	1709	85.9	29.4	909	0.532
TD005	FEMALE	23	1492	148.9	66.9	884	0.592
TD006	MALE	23	1773	80.9	25.7	944	0.532
TD007	FEMALE	56	1626	79.2	30.0	871	0.536
TD008	FEMALE	47	1560	55.8	22.9	812	0.521
TD009	FEMALE	67	1637	66.8	24.9	850	0.519
TD010	FEMALE	57	1655	58.7	21.4	913	0.552
TD011	MALE	30	1678	134.9	47.9	904	0.539
TD012	FEMALE	25	1616	56.9	21.8	876	0.542
TD013	FEMALE	48	1619	66.3	25.3	877	0.542
TD014	MALE	30	1743	61.9	20.4	918	0.527
TD015	MALE	35	1784	72.4	22.7	914	0.512
TD016	FEMALE	46	1757	125.8	40.8	921	0.524
TD017	FEMALE	64	1578	93.5	37.5	851	0.539
TD018	FEMALE	20	1661	70.2	25.4	862	0.519
TD019	FEMALE	41	1558	69.3	28.5	864	0.555
TD020	MALE	41	1655	69.5	25.4	854	0.516
TD021	MALE	20	1691	59.7	20.9	866	0.512
TD022	FEMALE	66	1577	71.8	28.9	830	0.526
TD023	MALE	69	1929	95.5	25.7	999	0.518
TD024	MALE	62	1744	95.7	31.5	929	0.533
TD025	MALE	34	1732	90.4	30.1	913	0.527
TD026	FEMALE	19	1646	67.8	25.0	891	0.541
TD027	FEMALE	19	1544	62.3	26.1	854	0.553
TD028	FEMALE	27	1768	82.8	26.5	919	0.520
TD029	MALE	23	1787	68.1	21.3	923	0.517
TD030	MALE	22	1685	63.1	22.2	908	0.539
TD031	FEMALE	60	1624	63.5	24.1	833	0.513
TD032	FEMALE	65	1482	83.0	37.8	813	0.549

* SH/S = ratio of sitting height to stature.

Subject	Gender	Age (yr)	Stature (mm)	Weight (kg)	BMI (kg/m^2)	Sitting Height (mm)	SH/S*
TD033	FEMALE	41	1644	88.1	32.6	859	0.523
TD034	FEMALE	59	1649	79.0	29.1	872	0.529
TD035	FEMALE	23	1501	66.4	29.4	801	0.534
TD036	FEMALE	68	1523	66.0	28.5	849	0.557
TD037	FEMALE	63	1549	54.4	22.7	819	0.529
TD038	MALE	32	1646	99.7	36.8	899	0.546
TD039	MALE	67	1828	84.2	25.2	916	0.501
TD040	MALE	62	1754	84.7	27.5	922	0.526
TD041	MALE	68	1750	100.0	32.7	932	0.533
TD042	MALE	23	1682	79.7	28.2	879	0.523
TD043	FEMALE	29	1662	52.9	19.1	867	0.522
TD044	MALE	62	1683	78.7	27.8	871	0.518
TD045	MALE	51	1633	69.1	25.9	855	0.524
TD046	MALE	42	1776	71.4	22.6	920	0.518
TD047	MALE	26	1711	62.2	21.2	870	0.508
TD048	FEMALE	62	1662	54.8	19.8	867	0.522
TD049	FEMALE	30	1590	61.9	24.5	853	0.536
TD050	FEMALE	26	1567	52.3	21.3	871	0.556
TD051	FEMALE	22	1702	71.3	24.6	902	0.530
TD052	FEMALE	18	1627	56.9	21.5	895	0.550
TD053	FEMALE	62	1597	117.4	46.0	841	0.527
TD054	FEMALE	63	1570	57.9	23.5	805	0.513
TD055	MALE	66	1634	95.2	35.7	880	0.539
TD056	FEMALE	65	1629	87.6	33.0	869	0.533
TD057	FEMALE	30	1705	100.5	34.6	941	0.552
TD058	FEMALE	20	1501	74.1	32.9	799	0.532
TD059	MALE	59	1694	83.6	29.1	879	0.519
TD060	FEMALE	36	1641	119.8	44.5	831	0.506
TD061	FEMALE	59	1550	84.2	35.0	861	0.555
TD062	FEMALE	49	1613	101.6	39.1	820	0.508
TD063	MALE	43	1775	117.2	37.2	911	0.513
TD064	FEMALE	30	1661	88.5	32.1	879	0.529
TD065	MALE	63	1755	100.5	32.6	930	0.530
TD066	MALE	59	1776	83.0	26.3	959	0.540
TD067	FEMALE	67	1595	100.2	39.4	825	0.517

* SH/S = ratio of sitting height to stature.

Subject	Gender	Age (yr)	Stature (mm)	Weight (kg)	BMI (kg/m^2)	Sitting Height (mm)	SH/S*
TD068	MALE	54	1756	116.7	37.8	929	0.529
TD069	MALE	27	1816	103.1	31.3	947	0.521
TD070	MALE	19	1919	92.0	25.0	987	0.514
TD071	MALE	44	1825	97.9	29.4	977	0.535
TD072	MALE	55	1835	112.7	33.5	954	0.520
TD073	MALE	55	1722	136.3	46.0	904	0.525
TD074	MALE	23	1863	78.8	22.7	942	0.506
TD075	FEMALE	36	1498	46.6	20.7	772	0.515
TD076	MALE	52	1648	81.5	30.0	842	0.511
TD077	FEMALE	63	1672	58.5	20.9	873	0.522
TD078	MALE	53	1736	94.6	31.4	914	0.526
TD079	FEMALE	58	1723	72.6	24.5	950	0.551
TD080	MALE	70	1880	108.7	30.7	940	0.500
TD081	MALE	55	1717	61.9	21.0	905	0.527
TD082	FEMALE	60	1565	108.3	44.2	828	0.529
TD083	FEMALE	60	1633	80.8	30.3	866	0.530
TD084	MALE	59	1738	64.4	21.3	919	0.529
TD085	MALE	23	1680	94.4	33.4	919	0.547
TD086	FEMALE	60	1645	115.4	42.6	883	0.537
TD087	MALE	22	1898	88.8	24.7	952	0.502

* SH/S = ratio of sitting height to stature.

Appendix D
Head CG Excursion Tables

Table D1
Head CG Excursion in Braking Trials, Sorted by Excursion in First Trial (mm)

	First Braking Event		Second Braking Event	
Subject	**Mean***	**Max**	**Mean***	**Max**
TD079	9.6	-71.1	-121.8	-135.2
TD070	-11.9	-110.2	-124.2	-137.2
TD062	-20.5	-54.0	37.9	-30.6
TD060	-25.8	-71.2	-60.7	-93.1
TD020	-27.2	-112.7	4.8	-74.7
TD033	-32.1	-118.4	-87.0	-145.9
TD044	-41.5	-87.9	-117.3	-142.7
TD038	-50.7	-123.2	-62.7	-95.0
TD022	-61.9	-106.6	-8.1	-60.9
TD061	-63.8	-71.6	-16.4	-77.3
TD009	-64.5	-123.5		
TD041	-66.8	-127.7	-24.9	-104.2
TD023	-76.1	-128.7	-88.6	-114.7
TD082	-78.2	-95.1	-110.8	-137.0
TD024	-81.1	-150.2	-89.2	-117.1
TD034	-81.3	-112.0	-106.6	-117.1
TD059	-84.9	-141.1	-83.2	-114.0
TD010	-92.9	-148.7		
TD037	-95.9	-155.0	-82.5	-154.8
TD054	-97.6	-118.5	-52.4	-81.6
TD012	-99.3	-157.2	-103.1	-155.4
TD036	-100.5	-120.2	-93.4	-134.2
TD066	-103.5	-121.1	-42.2	-81.4
TD045	-106.9	-148.2	-198.0	-246.0
TD055	-113.2	-154.2		
TD029	-115.1	-160.8	-83.5	-165.1
TD053	-115.1	-166.8	-119.7	-138.3
TD063	-118.4	-131.8	-89.8	-116.0
TD068	-118.8	-144.1	-113.3	-122.2
TD076	-120.4	-143.0	-58.1	-72.9
TD014	-124.2	-182.1	-187.9	-225.4
TD025	-128.3	-142.7	-114.0	-129.1
TD057	-129.0	-141.8	-103.1	-150.7
TD056	-129.1	-158.0	-103.5	-135.5
TD011	-129.2	-165.8	-46.1	-78.9
TD064	-130.2	-172.0		

* Mean during interval from 0.5 to 1.5 seconds

Table D1 (continued)

	First Braking Event		Second Braking Event	
Subject	**Mean***	**Max**	**Mean***	**Max**
TD083	-132.3	-167.6	-83.1	-115.7
TD004	-133.6	-163.5	-127.4	-151.5
TD074	-136.3	-156.3	-161.7	-189.8
TD065	-140.0	-152.0	-135.7	-159.3
TD085	-144.3	-161.3	-150.2	-175.1
TD046	-145.7	-176.8	-84.5	-132.8
TD042	-147.2	-168.7	-135.8	-167.5
TD086	-150.4	-180.9	-145.7	-170.6
TD013	-154.0	-168.0	-82.9	-151.4
TD072	-155.1	-184.6	-128.6	-142.3
TD048	-158.1	-191.0	-132.0	-146.0
TD080	-159.7	-175.7	-104.9	-131.7
TD078	-166.2	-204.0	-127.9	-158.4
TD047	-167.4	-197.1	-176.2	-195.0
TD077	-168.3	-193.2	-144.8	-192.3
TD039	-169.3	-197.7	-86.2	-126.3
TD026	-170.1	-183.2	-170.4	-196.3
TD031	-173.4	-200.2	-164.0	-220.8
TD002	-174.0	-195.2	-157.4	-164.3
TD028	-179.1	-210.8	-158.1	-201.7
TD058	-185.5	-212.2		
TD021	-189.7	-211.1	-149.5	-217.0
TD018	-192.8	-212.9		
TD017	-193.2	-198.6	-106.2	-148.3
TD043	-196.1	-229.8	-169.4	-224.1
TD016	-198.5	-208.0	-72.7	-111.7
TD019	-199.4	-211.1	-164.3	-205.1
TD032	-200.9	-215.1	-157.4	-187.3
TD001	-202.5	-214.9	-146.6	-260.9
TD035	-203.2	-238.7	-141.8	-175.2
TD071	-210.6	-232.6	-177.6	-213.9
TD069	-210.7	-222.8	-200.1	-215.8
TD084	-213.3	-222.5	-219.5	-227.9
TD050	-220.1	-248.4	-171.7	-196.3
TD049	-223.7	-236.7		
TD081	-228.5	-260.0	-156.2	-189.3
TD015	-229.2	-232.3	-161.8	-178.3
TD003	-240.0	-264.2	-182.6	-197.2
TD030	-255.4	-275.3	-227.1	-249.8
			20.5	-42.8

* Mean head CG excursion during interval from 0.5 to 1.5 seconds

Table D2
Mean and Maximum Head CG Excursions in Lane-Change and Turn-and-Brake Trials (mm)

	Lane Change*		Turn and Brake**	
Subject	**Mean**	**Max**	**Y Excursion (0.6 s)**	**X Excursion (2.8 s)**
TD036	-34.0	-47.9		
TD062	-34.1	-36.3	-34.0	7.3
TD067	-35.2	-56.2	-94.7	-3.8
TD061	-39.2	-64.6	-104.1	-53.1
TD011	-39.3	-47.3		
TD025	-49.2	-61.0	-81.4	-14.9
TD066	-56.5	-62.5	-110.8	-35.3
TD037	-59.2	-64.5	-67.0	-40.4
TD041	-64.6	-69.5	-124.4	-7.7
TD050	-73.7	-75.1	-130.1	-134.9
TD077	-73.9	-82.0	-137.1	-78.9
TD076	-75.3	-80.2	-92.3	-23.1
TD085	-78.1	-85.5	-90.9	-24.3
TD056	-78.8	-85.3	-142.4	-60.7
TD082	-81.1	-92.5	-91.0	-42.5
TD018	-82.2	-89.9		
TD043	-87.8	-96.5	-144.8	-88.8
TD084	-88.3	-100.4	-129.8	-62.9
TD015	-89.1	-106.5	-115.3	-82.7
TD083	-89.4	-94.1	-122.6	-64.8
TD014	-89.5	-108.3	-87.5	-94.8
TD042	-91.6	-100.6	-114.7	-74.2
TD044	-93.5	-124.9	-134.5	-66.0
TD080	-95.2	-117.0	-171.7	-39.4
TD072	-95.9	-101.5	-130.2	-77.8
TD047	-96.9	-105.2	-104.9	-47.9
TD060	-98.3	-110.6	-132.1	-93.1
TD035	-101.1	-102.8	-152.5	-130.3
TD078	-101.6	-108.6	-164.6	-28.0
TD048	-103.3	-110.8	-137.9	-64.1
TD055	-104.9	-120.2	-116.3	-142.6
TD045	-105.2	-146.1	-137.3	-108.7
TD033	-108.7	-122.5	-79.0	-27.3
TD009	-109.1	-115.0	-143.5	25.2
TD028	-110.9	-114.6	-150.5	-124.8
TD079	-111.1	-116.3	-140.8	-29.1
TD071	-114.0	-118.4	-147.8	-20.9
TD059	-114.2	-123.9		

* Mean Y-axis (lateral) head CG excursion from start between 0.4 and 0.9 seconds
** Head CG excursion from start at 0.6 (Y-axis) and 2.8 (X axis) seconds.

Table D2 (continued)

	Lane Change*		Turn and Brake**	
Subject	**Mean**	**Max**	**Y Excursion (0.6 s)**	**X Excursion (2.8 s)**
TD038	-116.7	-127.9	-98.6	-43.4
TD070	-117.2	-123.9	-158.4	-0.8
TD016	-118.7	-125.1	-125.3	-18.0
TD074	-122.9	-134.2	-97.3	-27.0
TD032	-129.7	-142.6	-105.6	-137.5
TD021	-133.1	-146.7	-181.0	3.8
TD046	-133.3	-154.5	-171.3	31.4
TD012	-136.1	-141.3	-118.8	-19.5
TD017	-137.2	-146.2	-141.6	-58.6
TD029	-138.8	-149.1	-132.5	-69.8
TD019	-140.5	-150.9	-153.9	-83.1
TD026	-140.5	-159.0	-140.3	-134.8
TD001	-144.6	-175.9		
TD057	-145.9	-155.7	-195.6	-10.7
TD003	-147.0	-161.9	-187.5	-57.5
TD065	-147.3	-161.0	-208.4	-149.5
TD004	-148.3	-166.0	-152.0	-5.2
TD030	-148.7	-168.5	-153.4	-73.4
TD069	-155.6	-158.8	-167.5	-171.0
TD034	-159.7	-163.5	-140.7	-32.5
TD023	-161.0	-180.5	-158.0	-55.7
TD002	-165.5	-176.2	-157.9	-101.1
TD039	-168.7	-174.0		
TD031	-225.7	-231.2	-182.7	-141.6
TD010			-165.9	-57.4
TD020			-43.3	-21.5
TD022			-81.3	-7.5
TD024			-103.3	-46.9
TD049			-99.0	-89.7
TD051			-165.3	-61.5
TD053			-102.0	-75.6
TD054			-108.2	-55.3
TD058			-112.4	-94.4
TD063			-164.8	-84.9
TD064			-109.7	-117.5
TD068			-151.8	-27.5
TD081			-218.5	-47.8
TD086			-149.7	-42.7

* Mean Y-axis (lateral) head CG excursion from start between 0.4 and 0.9 seconds

** Head CG excursion from start at 0.6 (Y-axis) and 2.8 (X axis) seconds.